


Plant immunity suppressor SKRP encodes a novel RNA-binding protein that targets exon 3' end of unspliced RNA

Ling Chen^{1,2} , Zhihui Xu³ , Jie Huang¹ , Haidong Shu¹ , Yufan Hui^{2,4} , Danling Zhu² ,
Yufeng Wu³ , Suomeng Dong¹  and Zhe Wu² 

¹Department of Plant Pathology, Key Laboratory of Integrated Management of Crop Diseases and Pests (Ministry of Education), and The Key Laboratory of Plant Immunity, Nanjing Agricultural University, Nanjing, 210095, China; ²Key Laboratory of Molecular Design for Plant Cell Factory of Guangdong Higher Education Institutes, Institute of Plant and Food Science, Department of Biology, School of Life Sciences, Southern University of Science and Technology, Shenzhen, 518055, China; ³National Key Laboratory for Crop Genetics and Germplasm Enhancement, Bioinformatics Center, Academy for Advanced Interdisciplinary Studies, Jiangsu Collaborative Innovation Center for Modern Crop Production, Nanjing Agricultural University, Nanjing, 210095, China; ⁴School of Computing Sciences, University of East Anglia, Norwich, NR4 7TJ, UK

Authors for correspondence:
Suomeng Dong
Email: smdong@njau.edu.cn

Zhe Wu
Email: wuz@sustech.edu.cn

Received: 1 July 2023
Accepted: 1 August 2023

New Phytologist (2023) 240: 1467–1483
doi: 10.1111/nph.19236

Key words: intron retention, *Phytophthora*, plant immunity, RNA-binding protein, SKRP, splicing.

Summary

- The regulatory roles of RNA splicing in plant immunity are emerging but still largely obscure. We reported previously that *Phytophthora* pathogen effector Avr3c targets a soybean protein SKRP (serine/lysine/arginine-rich protein) to impair soybean basal immunity by regulating host pre-mRNA alternative splicing, while the biochemical nature of SKRP remains unknown.
- Here, by using Arabidopsis as a model, we studied the mechanism of SKRP in regulating pre-mRNA splicing and plant immunity.
- AtSKRP confers impaired plant immunity against *Phytophthora capsici* and associates with spliceosome component PRP8 and splicing factor SR45, which positively and negatively regulate plant immunity, respectively. Enhanced crosslinking and immunoprecipitation followed by high-throughput sequencing (eCLIP-seq) showed AtSKRP is a novel RNA-binding protein that targets exon 3' end of unspliced RNA. Such position-specific binding of SKRP is associated with its activity in suppressing intron retention, including at positive immune regulatory genes *UBP25* and *RAR1*. In addition, we found AtSKRP self-interact and forms oligomer, and these properties are associated with its function in plant immunity.
- Overall, our findings reveal that the immune repressor SKRP is a spliceosome-associated protein that targets exon 3' end to regulate pre-mRNA splicing in Arabidopsis.

Introduction

As a key step of the gene expression pipeline, pre-mRNA splicing exerts important regulatory functions by determining certain combinations of sequences that present at individual mRNA. The splicing reaction is catalyzed by a giant complex known as spliceosome, which is composed of five core small nuclear ribonucleoprotein complexes (U1, U2, U4, U5, and U6 snRNPs) and lots of other RNA-binding proteins such as serine/arginine-rich (SR) proteins and U2 auxiliary factors (U2AF) (Jurica & Moore, 2003; Wang & Brendel, 2004; Bessonov *et al.*, 2008; Will & Luhrmann, 2011; Shi, 2017). While spliceosome itself is sufficient for splicing, evidence in yeast, animals, and plants suggests splicing and transcription are tightly coupled such that the majority of splicing reaction occurs on chromatin during transcription (Bentley, 2014; Li *et al.*, 2020; Zhu *et al.*, 2020). Notably, although the core components of the spliceosome are generally conserved, the auxiliary factors of the spliceosome are considerably variable among different species (Wang &

Brendel, 2004; Kastner *et al.*, 2019; Yan *et al.*, 2019). For example, the SR protein family is expanded from nine members in humans to 19 members in Arabidopsis, many of which have shown plant specificity at the primary sequence level to a certain extent (Barta *et al.*, 2010). The identity and functions of the auxiliary factors of the spliceosome in plants remain elusive.

The regulatory power of splicing is best demonstrated by alternative splicing (AS), through which one gene encodes multiple isoforms of mRNAs upon external or internal cues (Staiger & Brown, 2013). Intron retention (IR), exon skipping (ES), usage of alternative 5' and 3' splice sites (A5SS and A3SS), and mutually exclusive exons (MXE) are major types of AS (Marquez *et al.*, 2015). It is estimated that *c.* 60% of mRNA transcripts from Arabidopsis and soybean undergo AS (Marquez *et al.*, 2012; Shen *et al.*, 2014). In addition to AS, the tight cooperativity between splicing and transcription also renders splicing a critical step in monitoring the RNA quality during transcription (Naftelberg *et al.*, 2015; Garland & Jensen, 2020). For example, defective splicing leads to failure of deposition of exon junction

complex, which is critical for nonsense-mediated mRNA decay (Kalyna *et al.*, 2012; Lee *et al.*, 2020).

Accumulating evidence suggests splicing is an important regulatory layer in plant immunity (Mandadi & Scholthof, 2015; Rigo *et al.*, 2019; Huang *et al.*, 2020). The plant has evolved a sophisticated two-layer immune system to fight against pathogens (Jones & Dangl, 2006). Pattern-triggered immunity (PTI) describes the first layer of basal immune response triggered by pathogen-associated molecular patterns such as elongation factor TU (EF-Tu), flagellin, and chitin (Couto & Zipfel, 2016). Effector-triggered immunity (ETI) represents the second layer of immunity through which the plant utilizes resistance (R) proteins to recognize cognate pathogen avirulence (Avr) proteins and trigger a stronger immune response (Cui *et al.*, 2015). The host transcriptome often undergoes extensive reprogramming upon pathogen infection, including AS (Huang *et al.*, 2017; Bjornson *et al.*, 2021). It was reported that >90% of transcripts undergo AS in *Arabidopsis* upon infection by *Pseudomonas syringae* (Howard *et al.*, 2013). Intriguingly, many R genes undergo AS, such as *RPS4* (Resistance to *pseudomonas syringae* 4) in *Arabidopsis*, *N* gene in Tobacco, and *RCT1* (Resistance to *C. trifolii* race 1) in Medicago (Yang *et al.*, 2014). In many cases, the ratio between different isoforms alters upon pathogen infection, and expression of only one isoform does not fully compensate the mutant phenotype (Dinesh-Kumar & Baker, 2000; Zhang, 2003; Tang *et al.*, 2013), suggesting the functional importance of the AS for immunity.

Many splicing-related proteins are found to be important for plant immunity. SNC1 (Suppressor of *npr1-1*, constitutive 1) encodes an important immune signaling regulator such that *snc1* exhibits constitutive activation of defense signaling without pathogen infection (Li *et al.*, 2001; Zhang *et al.*, 2003). Interestingly, screening of mutants that modify *snc1* phenotype leads to the identification of 13 MOS (Modifier of *snc1*) genes, among which a few are splicing-related proteins (Palma *et al.*, 2005, 2007; Zhang *et al.*, 2005; Zhang & Li, 2005; Goritschnig *et al.*, 2007, 2008; Wiermer *et al.*, 2007; Cheng *et al.*, 2009; Germain *et al.*, 2010; Li *et al.*, 2010; Xu *et al.*, 2011, 2012). For example, MOS4 is a homolog of human spliceosome-associated protein BCAS2 (Breast cancer-amplified sequence 2; Palma *et al.*, 2007). MOS4 interacts with CDC5 (Cell division cycle 5) and PRL1 (Pleiotropic regulatory locus 1) to form a spliceosome-associated complex termed the MOS4-associated complex (MAC; Palma *et al.*, 2007). MOS4, MAC3A/3B (Prp19 homolog), MOS12 (An SR protein homolog), and MOS14 (Transportin of SR) are reported to regulate splicing of SNC1 and RPS4 (Palma *et al.*, 2007; Monaghan *et al.*, 2009; Xu *et al.*, 2011, 2012). While the data highlight the profound involvement of spliceosome-associated proteins in plant immunity, the exact working mechanism of these proteins during splicing reactions remains elusive.

We previously studied an avirulence effector PsAvr3c secreted by soybean pathogen *Phytophthora sojae*, which resulted in the identification of one target protein in soybean named SKRP (Huang *et al.*, 2017). PsAvr3c protects SKRP from degradation mediated by 26S proteasome (Huang *et al.*, 2017). Further analysis showed that SKRPs are negative regulators of plant immunity

in soybean and tobacco (*Nicotiana benthamiana*; Huang *et al.*, 2017). SKRP is associated with several soybean spliceosome components including GmSR45, GmU2AF35, and GmU1-70K, and regulates pre-mRNA AS of hundreds of genes, including several defense-related genes (Huang *et al.*, 2017).

In this study, we dissected the molecular function of SKRP in detail by using *Arabidopsis* as a model plant. Like its homolog in soybean, *Arabidopsis* SKRP functions to negatively regulate plant immunity. AtSKRP forms polymers *in vivo*, in part attributes to its C-terminal monkey tail domain. Unexpectedly, we found AtSKRP specifically binds ssRNA *in vitro*, suggesting it is an RNA-binding protein. The further *in vivo* eCLIP-seq analysis confirmed this hypothesis, such that AtSKRP specifically targets exon and intron 3' end in the unspliced pre-mRNAs. AtSKRP associates with core spliceosome components PRP8 (pre-mRNA processing factor 8) and splicing factor SR45, which function to promote and suppress plant immunity, respectively. Lastly, we present evidence that AtSKRP, in conjunction with its RNA-binding capability, governs splicing, thereby facilitating the splicing of crucial genes involved in plant immunity regulation, such as *UBP25* (Ubiquitin-specific Protease 25) and *RAR1* (Required for *Mla12* Resistance 1). Intriguingly, the presence of the unspliced transcripts of *UBP25* and *RAR1* negatively impact plant immunity. Overall, we uncovered the biochemical nature of plant immune suppressor SKRP and revealed its function in the context of pre-mRNA splicing in *Arabidopsis*.

Materials and Methods

Plant material and growth condition

All *Arabidopsis* plants used in this study are in *Columbia* (Col-0) background except for *prp8*. Seeds were kept in the dark for 3 d at 4°C for stratification. *Arabidopsis thaliana* plants were grown on half-strength Murashige & Skoog plates containing 1% sucrose at 22°C under a 16 h : 8 h, light : dark cycle.

Mutant plant *atskrp-t* (SALK_054359C) was originally from *Arabidopsis* Biological Resource Center (ABRC). For generating knockout mutants using the CRISPR/Cas9 system, target sequences were designed at <http://skl.scau.edu.cn/targetdesign/> (Xie *et al.*, 2017) and the primers used for construction and genotyping are listed in Supporting Information Dataset S1. The CRISPR/Cas9 constructs were made according to the methods described previously (Wang *et al.*, 2015). The mutant *ubp25* (SALK_111336C), *rar1-1* (SALK_089054C), *rar1-2* (SALK_013489C), and *u2af65a* (SALK_144790C) were purchased from AraShare (Fuzhou, China). *cdc5-1* (SAIL_207_F03), *sr45-1* (SALK_004132), and *prp8-6* have been described previously (Ali *et al.*, 2007; Palma *et al.*, 2007; Marquardt *et al.*, 2014). The primers used for genotyping are presented in Dataset S1.

For overexpression, CDS of AtSKRP and eGFP were cloned into the destination vector pCAMBIA1300-nLUC (linearized by digested with KpnI and PstI; Chen *et al.*, 2008) by using ClonExpress™ MultiS one-step cloning kit (C113-01; Vazyme, Nanjing, China). The *35S::GFP-AtSKRP* construct was transformed into the *atskrp-t* mutant plants by floral dip (Clough &

Bent, 1998). The transformants were identified through antibiotic selection and PCR confirmation, after which the T3 generation was generated for phenotype analysis.

Microbe cultivation and inoculation

Phytophthora capsici (Pc35) strain was routinely maintained on a 10% V8 solid medium at 25°C in the dark. For infection assays, 10-d-old seedlings were infected by *P. capsici* zoospore suspension (containing *c.* 15 000 zoospores ml⁻¹). The infected samples were maintained in the dark at 25°C and at high humidity for 24 h before the assessment of infection. The infection assays were assessed by determining the *P. capsici* biomass (the ratios of *P. capsici* to Arabidopsis DNA) at 24 h postinoculation (hpi) by using genomic DNA quantitative PCR, for which the *P. capsici* *Actin* gene and Arabidopsis *UBC9* gene (primers in Dataset S1) were amplified. The infected samples were stained using Trypan Blue Staining Kit (E607320; Sangong Biotech, Shanghai, China) and then transferred into ethanol and incubated at 25°C for 24 h before observation. For 4-week-old seedling, *P. capsici* mycelia were inoculated on leaves. The photographs were taken at 48 hpi under UV light. *Pst* DC3000 infection assay was performed as reported previously (Kong *et al.*, 2021).

Callose deposition

The infected leaves were stained with Plant Callose Staining Solution (cat. G4805; Solarbio, Beijing, China) according to the manufacturer's instructions. More details can be found in Methods S1.

Yeast two-hybrid assays

The yeast two-hybrid (Y2H) assay was carried out as previously reported (Huang *et al.*, 2017). More details can be found in Methods S2.

DAB staining

The infected leaves were stained with DAB solution, as described in Methods S3.

GST-pull down

To prepare GST-fused and His-fused AtSKRP, CDS of AtSKRP was cloned into pGEX4T-1 (GST tag) and pET32a (His tag), after which the resulting constructs were transformed into *Escherichia coli* Rosetta for protein expression. More details can be found in Methods S4.

Electrophoretic mobility shift assay

GST-AtSKRP or GST was incubated with biotin-labeled probe in binding buffer. The RNA–protein complexes were resolved on native gel and detected with Chemiluminescent Nucleic Acid Detection Module (Thermo Fisher Scientific, Waltham, MA, USA). More details can be found in Methods S5.

Agrobacterium-mediated transient assay

The *Agrobacterium* resuspension containing CDS of *UBP25* and *RAR1* was hand-infiltrated into *N. benthamiana* leaves. The leaf samples were infected at 36 hpi. More details can be found in Methods S6.

Bimolecular fluorescence complementation assay

Coding sequence of AtSKRP and Pi04314 (negative control protein) was cloned into both the vector pCL112 (YFP^N) and pCL113 (YFP^C). Bimolecular fluorescence complementation (BiFC) was conducted using 4-wk-old *N. benthamiana* leaves, following the protocol published previously (Wu *et al.*, 2016). More details can be found in Methods S7.

Gel filtration

GST-AtSKRP, mutations GST-AtSKRP^{ΔOR5}, and GST-AtSKRP^{ΔOR10} were purified by using a Superose 6 increase 10/300 GL (29-0915-96; GE Healthcare, Barrington, IL, USA) column. More details can be found in Methods S8.

Polymer detection

GFP-AtSKRP, mutants GFP-AtSKRP^{ΔOR5}, and GFP-AtSKRP^{ΔOR10} were lysed followed immunoprecipitation with GFP-Trap Magnetic Agarose (gtma-20; ChromoTek, Martinsried, Germany). The resulting beads were washed, followed by heat or detergent treatment. The proteins were released from beads and detected by immunoblot with anti-GFP antibody (1 : 5000, Ab290; Abcam, Cambridge, UK). More details can be found in Methods S9.

Yeast protein extraction

The yeast protein extraction is described previously (Zhang *et al.*, 2011). More details can be found in Methods S10.

RNA immunoprecipitation

RNA immunoprecipitation was performed as described previously (Yang *et al.*, 2022). Ten-day-old seedlings were cross-linked with 1% formaldehyde (FA). Samples were subjected to immunoprecipitation with an anti-GFP antibody (Ab290; Abcam) and protein A beads (Dynabeads; Thermo Fisher Scientific). The RNA was purified and then used for reverse transcription with gene-specific primers. More details can be found in Methods S11.

RNA isolation and RT-qPCR

RNA was isolated using the HiPure Plant RNA Mini Kit (Magen, Guangzhou, China) according to the manufacturer's instructions and used for cDNA synthesis and qPCR as described previously (Yang *et al.*, 2022). More details can be found in Methods S12.

RNA sequencing library construction

RNAs isolated from Col-0, *atskrp-t* (0 and 24 hpi), and *35S::GFP-AtSKRP* were used to construct RNA-Seq libraries by using the dUTP method and with a NEBNext Ultra II Directional RNA Library Prep Kit for Illumina (E7760S; NEB, Ipswich, MA, USA) following the manufacturer's protocol. More details can be found in Methods S13.

eCLIP-seq

eCLIP-seq was performed as described previously with modifications (Huppertz *et al.*, 2014; Van Nostrand *et al.*, 2016; Meyer *et al.*, 2017; Zhu *et al.*, 2020). In brief, 10-d-old plants were crosslinked with UV (245 nm) light at 600 mJ cm^{-2} . Samples were lysed with iCLIP lysis buffer (50 mM Tris-HCl, pH 7.4, 100 mM NaCl, 1% NP-40, 0.1% SDS, 0.5% sodium deoxycholate, 2 mM DTT, 2× protease inhibitor (Roche), 0.8 u l^{-1} Recombinant RNasin[®] RNase inhibitor (Promega)), digested by RNase I (Thermo Fisher Scientific), and then sonicated. After Anti-GFP antibody (Ab290; Abcam) immunoprecipitation, high (1 M NaCl)- and low-salt washes were performed, followed by RNA dephosphorylation with FastAP (Thermo Fisher Scientific) and T4 PNK (Thermo Fisher Scientific) and 3' RNA adaptor ligation with T4 RNA ligase (NEB). Ten percent of IP samples were separated on a NuPAGE[™] 4–12% Bis-Tris protein gel and detected by HRP anti-GFP (1:2500, Ab190584; Abcam) immunoblot. The remainder of 90% IP samples was run on the same protein gel and transferred to nitrocellulose membranes, after which the region from the protein size to 75 kDa above protein size was excised from the membrane, treated with proteinase K (Thermo Fisher Scientific) to release RNA. The resulting RNA was further purified. Reverse transcription was then performed with Maxima H Minus Reverse Transcriptase (Thermo Fisher Scientific), followed by cDNA purification and a 3' DNA adaptor ligation with T4 RNA ligase (NEB). qPCR was then used to determine the required amplification, followed by PCR with Q5 Hot-Start DNA polymerase (NEB) and low-melting-point agarose gel electrophoresis to select fragments from 175 to 400 bp for pair-end Illumina (PE150) sequencing (Illumina, San Diego, CA, USA).

Immunoprecipitation and mass spectrometry

Ten-day-old seedlings powder was lysed with TAP buffer (20 mM Tris-HCl, pH 8, 150 mM NaCl, 2.5 mM EDTA, 1% Triton X-100, 5% Glycerol, 3× protease inhibitor (Roche)), followed by sonication, and then subjected to immunoprecipitation with an anti-GFP antibody (Ab290; Abcam) and protein A beads (Dyna-beads; Thermo Fisher Scientific). After immunoprecipitation, the beads were washed with TAP buffer and TAP-Triton X-100 buffer (20 mM Tris-HCl, pH 8, 150 mM NaCl, 2.5 mM EDTA, 5% Glycerol) until no bubbles. Ten of the resulting samples were loaded on an 8% SDS-PAGE gel and followed by silver staining.

For mass spectrometry analysis, 90% of protein samples from the above steps were loaded into a NuPAGE[™] 10%, Bis-Tris

(NP0301BOX; Invitrogen) gel and run until the loading dye migrated 3 cm from the well. The band (except the heavy and light chains of the antibody) was cut out as a whole for mass spectrometry analysis. GFP-AtSKRP LFQ (label-free quantitation) values were compared with those of the GFP-only control by Student's *t*-test. Significantly enriched proteins bound by AtSKRP were further analyzed and categorized manually.

For co-immunoprecipitation, samples were lysed as above and then subjected to immunoprecipitation with GFP-Trap Magnetic Agarose, followed by washing with TAP buffer and TAP-Triton X-100 buffer. The resulting samples were detected by anti-PRP8 and anti-BRR2 antibody immunoblot.

Reads pre-processing and alignment

Raw reads from mRNA and eCLIP sequencing data were processed by TRIM-GALORE (v.0.4.1) to remove adaptors, Ns, and low-quality reads. For eCLIP data, the first 10 random bases at the 5' end of read2 were trimmed and moved to the read header for marking PCR duplicates. Clean reads were then mapped to the Arabidopsis Col-0 reference genome (TAIR 10) using HISAT2 (v.2.1.0; Kim *et al.*, 2019) with Araport11 annotation. The parameters of HISAT2 were modified (--no-softclip --score-min -L, 0.6, -0.6) to obtain more mapped reads for calling crosslinking sites. Multiple mapped reads were filtered with in-house PYTHON script. Only unique reads were used for downstream analysis.

Identification of alternative-splicing events

The differentially spliced introns between WT and mutant were identified as previously described using Fisher's test (Deng *et al.*, 2010; Wu *et al.*, 2016). In brief, the number of reads for each exon-intron-exon combination was counted from mRNA datasets of WT and *atskrp*^{-/-} mutant lines by using HTSEQ (Anders *et al.*, 2015). A 2×2 contingency table was filled by intron reads and its flanking exons reads, and then Fisher's test was performed to identify alternative-splicing events. After Benjamini-Hochberg's adjustment, the significant alternative-splicing events should meet the requirement that the false discovery rate was < 0.05 .

eCLIP data analysis

According to the protocol of eCLIP experiment, peaks and cross-linking sites were identified by PIPE-CLIP (Chen *et al.*, 2014) with parameters '-l 20 -m 10 -c 3 -r 0 -M 0.05 -c 0.05'. The predicted binding sites (FDR < 0.05) that overlapped with peaks (FDR < 0.05) were extracted and referred as 'reliable xlsites'. Then, we merged the binding sites called from each replicate and used for downstream analysis.

Motif discovery

MEME-CHIP (Machanick & Bailey, 2011) was used to find motifs with default setting. The detail is described in Methods S14.

Results

AtSKRP confers impaired disease resistance in Arabidopsis

We wondered whether it is possible to dissect the molecular mechanism of SKRP in modulating splicing and plant immunity by using Arabidopsis as a model. BLAST search together with phylogenetic analysis showed orthologs of GmSKRP exist in various plant species, from bryophytes to monocots and dicots, including Arabidopsis (Fig. 1a), suggesting SKRP family proteins are likely to evolve early during land plant evolution. Multiple sequence alignment revealed high sequence similarity among SKRP orthologs, especially for their C terminus (Fig. S1). Specifically, Arabidopsis SKRP (AtSKRP) has 80% identity of its ortholog in soybean, indicating their functions are likely to be conserved in both species. To test such a hypothesis, we obtained T-DNA insertional mutant and multiple CRISPR mutants of SKRP (Fig. 1b). *AtSKRP* expression was largely eliminated in *SALK_054359C* (*atskrp-t*; Fig. S2a), while the genomic fragments are depleted in two CRISPR mutants *atskrp-16* (–95-bp depletion) and *atskrp-37* (–1425-bp depletion), both alleles display premature stop codon within the first exon of SKRP (Fig. S2b,c). An SKRP overexpression line (*35S::GFP-AtSKRP*) in the *atskrp-t* background was also generated (Figs 1c, S2a). No morphological defect under normal growth conditions was observed in the mutant lines or the overexpression line at the seedling and bolting stage (Fig. S2d,e), suggesting SKRP is not essential for normal plant development. An infection assay with *P. capsici* isolate Pc35 on 10-d-old seedlings or 4-wk-old leaves showed that all three mutant alleles display enhanced resistance to *P. capsici* than Col-0. By contrast, the overexpression line displays decreased resistance to *P. capsici* than Col-0 (Fig. 1d–g). Moreover, the callose deposition and ROS production were significantly induced in infected *atskrp* and reduced in infected *GFP-AtSKRP* (Figs 1h,i, S3a). To test whether AtSKRP participates in plant defense generally, we inoculated *atskrp* and *GFP-AtSKRP* with pathogenic bacteria *P. syringae* pv tomato (*Pst*) DC3000, *atskrp* was found to be more resistant, and *GFP-AtSKRP* was more susceptible than the wild-type plants (Fig. 1j), suggesting that AtSKRP negatively regulates plant resistance against *Pst* DC3000. The absence of morphological phenotype in *atskrp* also suggests that unlike many other immunity regulators such as *snc2-1D*, loss of SKRP does not activate autoimmunity but rather increases the immunity upon pathogen infection. Consistently, we found autoimmunity marker PR5 was only activated at 0.5 h after infection (Fig. S3b). Taken together, similar to GmSKRP, AtSKRP negatively regulates plant immunity.

AtSKRP self-interact and forms oligomer *in vivo*, and these properties are associated with its function in plant immunity

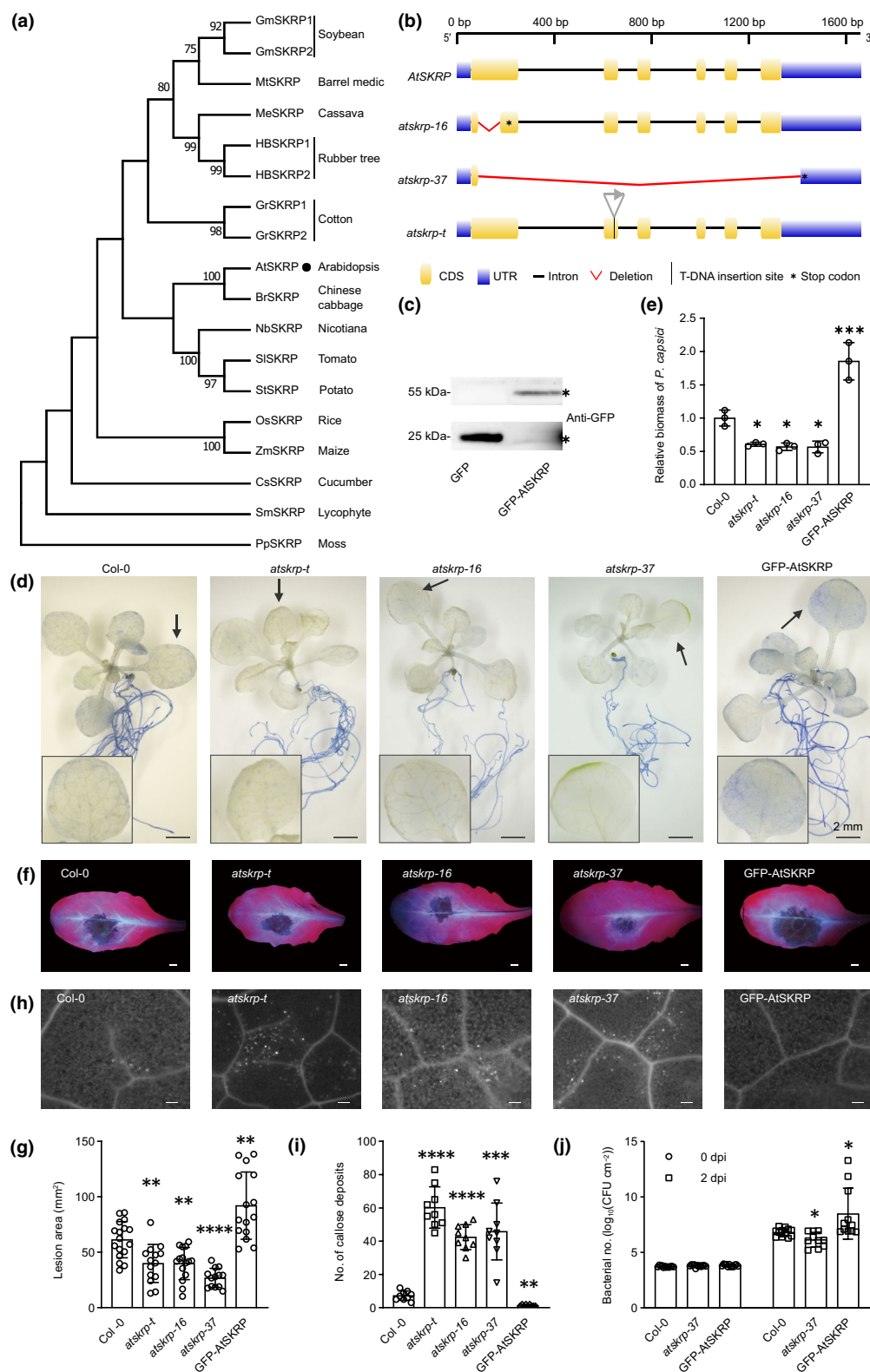
To understand the biochemical property of AtSKRP, we analyzed its amino acid sequence. The majority of AtSKRP is predicted to be disordered based on the Predictor of Natural Disordered Regions (PONDR; Fig. 2a). Notably, the C-terminal end

(aa 168–177, CE) of AtSKRP is predicted to be folded and has similarities to the monkey tail domain, a domain often responsible for protein–protein interactions (Moreno-Morcillo *et al.*, 2011). Consistently, through Y2H assay, we found AtSKRP can interact with itself in a fashion requiring its CE (Figs 2b, S4a). Specifically, depletion of either aa 168–172 (Δ OR5) or aa 168–177 (Δ OR10) disrupts the self-interaction of SKRP (Fig. 2b), while the CE of AtSKRP alone is unable to mediate the interaction with the CE itself (Fig. 2b). Thus, CE of AtSKRP is required but not sufficient to mediate the self-interaction of AtSKRP. Consistent with the observation in yeast, *in vitro* purified His-tagged SKRP can interact with GST-tagged SKRP (Fig. S4b), indicating SKRP can interact with itself directly.

The observed self-interaction in yeast and *in vitro* drives us to test whether this is also the case *in vivo*. As we expected, the self-interaction of AtSKRP can be observed in *N. benthamiana* epidermal cell through BiFC assay (Fig. S4c). In addition, confocal imaging of GFP-AtSKRP in Arabidopsis leaf revealed AtSKRP localized into the nucleus and displays a puncta-like localization pattern, indicating possible higher-order interactions among many different AtSKRP molecules (Fig. S4d). Consistently, the western blot of immunoprecipitated GFP-AtSKRP in Arabidopsis showed multiple bands corresponding to oligomeric AtSKRPs (Fig. 2c), indicating AtSKRPs form oligomers *in vivo*. The oligomers of SKRP can also be detected in the *in vitro* purified GST-SKRPs by using gel filtration (Fig. S5a). Intriguingly, the *in vivo* AtSKRPs oligomers can be observed after separating samples on the denatured gel (see Methods S1–S14), and such oligomers are resistant to RNase A, detergent (Triton X-100 and deoxycholate), and chaotropic salt (urea; Fig. 2c). Therefore, AtSKRP presents in oligomeric forms that are highly stable *in vivo*.

Next, given Δ OR5 or Δ OR10 disrupt the self-interaction of AtSKRP in yeast, we tested whether these mutations could also disrupt the oligomer formation of AtSKRP in Arabidopsis. We made Δ OR5 or Δ OR10 mutant constructs on the basis of *35S::GFP-AtSKRP* and transformed such constructs into *skrp* background. Several T3 homozygous lines were selected for further analysis. Compared with *35S::GFP-AtSKRP*, although the oligomers can still be observed, the ratio of monomer is significantly increased in Δ OR5 and Δ OR10 (Figs 2d,e, S6). Consistently, the oligomers of GST-SKRPs were also disrupted in Δ OR5 and Δ OR10 mutants as revealed by gel filtration (Fig. S5a–c). In addition, unlike *35S::GFP-AtSKRP*, overexpression of either Δ OR5 or Δ OR10 is unable to complement the increased resistance to *P. capsici* of *skrp* (Fig. 2f). Taken together, the above data suggest the AtSKRP self-interact and form oligomer *in vivo*, and such properties are tightly associated with its function in plant immunity.

Similar to AtSKRP, GmSKRPs also have similarly disordered N-terminal region and a C-terminal monkey tail-like domain (Figs S1, S7a). Consistently, we found GmSKRP can also interact with itself, requiring its monkey tail-like domain (Fig. S7b–d). Transient overexpression of the Δ OR10 mutant of GmSKRP1 in *N. benthamiana* leaves decrease the lesion size upon *P. capsici* infection (Fig. S7e–g). Thus, the self-interaction property of SKRP is conserved between Arabidopsis and soybean.



AtSKRP binds ssRNA specifically *in vitro*

Given SKRP in soybean was reported to regulate pre-mRNA splicing (Huang *et al.*, 2017), we wondered whether SKRP can function through the association with RNA. Indeed, there is a large

proportion of positively charged amino acids within the disordered region of SKRP, suggesting this protein may have the potential to interact with nucleic acids. In consistent with such a hypothesis, we noticed a significant amount of RNA, rather than DNA, and co-purified with GmSKRP when we purified the

Fig. 1 AtSKRP negatively regulates immunity against *Phytophthora capsici* in Arabidopsis. (a) Phylogenetic analysis of SKRPs from different plant species. Soybean – *Glycine max* (GmSKRP1, Glyma.03G234200 and GmSKRP2, Glyma.19G231600), barrel medic – *Medicago truncatula* (MtSKRP, Medtr7g112600), cassava – *Manihot esculenta* (MeSKRP, Manes.08G115600), rubber tree – *Hevea brasiliensis* (HBSKRP1, HBR1118G007 and HBSKRP2, HBR2617G049), cotton – *Gossypium raimondii* (GrSKRP1, Gorai.004G238900 and GrSKRP2, Gorai.007G301900), cucumber – *Cucumis sativus* L. (CsSKRP, Cucsa.181730), *Arabidopsis thaliana* (AtSKRP, AT5G27860), Chinese cabbage – *Brassica rapa* (BrSKRP, Brara.F02839), tomato – *Solanum lycopersicum* (SlSKRP, Solyc01g099930.2), potato – *Solanum tuberosum* (StSKRP, PGSC0003DMT400063724), *Nicotiana benthamiana* (NbSKRP, Niben101Scf00369g18022), lycophyte – *Selaginella moellendorffii* (SmSKRP, SMO367G0406), rice – *Oryza sativa* (OsSKRP, LOC_Os12g36740.1), maize – *Zea mays* (ZmSKRP, Zm00001d023824), and moss – *Physcomitrella patens* (PpSKRP, Pp3c11_23030V3.1). Values around the branches indicate bootstrap support > 70. AtSKRP is marked with a black circle. (b) Schematic presentation of different *atskrp* mutant alleles. *atskrp-16* and *atskrp-37* are genomic deletion mutants generated by CRISPR. Both mutants harbor premature stop codon as indicated by asterisk. *atskrp-t* is a T-DNA insertion mutant. (c) Western blot detection of GFP-AtSKRP protein in 35S:GFP-AtSKRP *skrp* transgenic line by using anti-GFP antibody. The position of expected protein bands is highlighted by the black asterisk. (d) Multiple alleles of *skrp* showed enhanced resistance to *P. capsici* isolate Pc35 while 35S:GFP-AtSKRP *skrp* showed enhanced susceptibility to *P. capsici* in 10-d-old seedlings. Image was taken at 24 h postinoculation (hpi); Bar, 2 mm. (e) The degree of *P. capsici* colonization at 24 hpi in 10-d-old seedlings. The relative biomass of *P. capsici* was determined by qPCR. In DNA samples, ratios of *P. capsici* Actin over Arabidopsis UBC9 were calculated and further normalized to such values in Col-0. Error bars indicate SD over three biological replicates. Asterisks indicate significant differences (*, $P < 0.05$; ***, $P < 0.001$). (f) *skrp* showed enhanced resistance to *P. capsici* while 35S:GFP-AtSKRP *skrp* showed enhanced susceptibility to *P. capsici* in 4-wk-old seedlings. Photographs were taken at 48 hpi under UV light. Bar, 2 mm. (g) Lesion area of infected leaves in (f). Lesion areas were measured at 48 hpi. Means and SD from separate measurements are shown (**, $P < 0.01$; ****, $P < 0.0001$). (h) Callose deposition in leaves infected with *P. capsici* zoospores. Representative micrographs of infected leaves that were inoculated with *P. capsici* zoospores stained by aniline blue. Bar, 100 μ m. (i) Number of callose deposits per microscopic field was quantitated. The data are mean \pm SD of the number of callose deposits per microscopic field (**, $P < 0.01$; ***, $P < 0.001$; ****, $P < 0.0001$, compared with Col-0). (j) The *skrp* mutant showed decreased susceptibility to *Pst* DC3000 while 35S:GFP-AtSKRP *skrp* showed enhanced susceptibility to *Pst* DC3000. Four-week-old plants were hand-inoculated with bacterial suspension. Bacterial growth was measured at 0- and 2-d postinoculation (dpi). Means and SD from separate measurements are shown (*, $P < 0.05$).

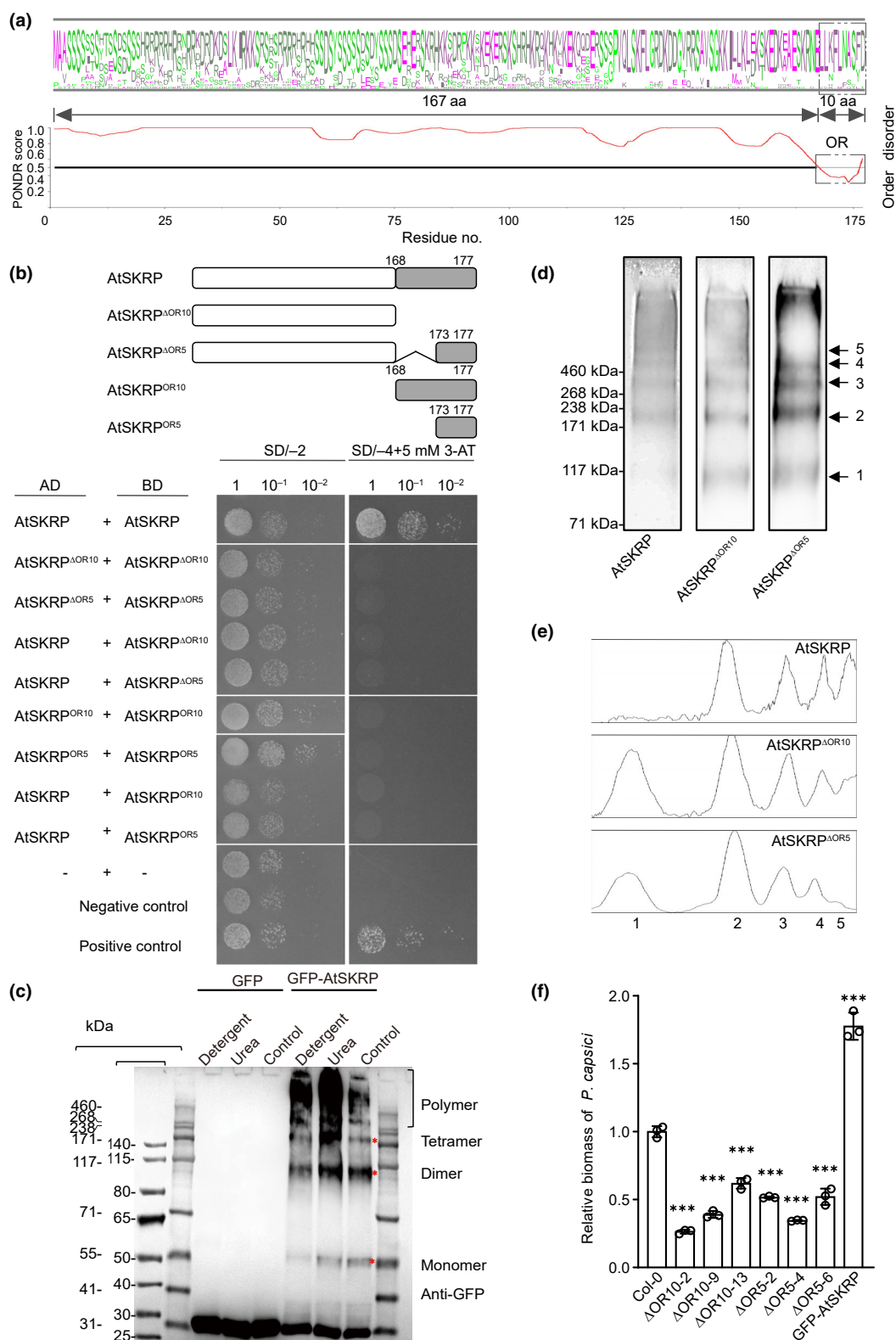
recombinant GmSKRP from *E. coli* (Fig. S8a). Consistently, strong UV 260 absorbance was observed when we purify the GST-AtSKRP from *E. coli* (Fig. S5a). Next, we tested whether SKRP can directly interact with nucleic acids *in vitro* by using electrophoretic mobility shift assay. In this assay, AG-rich or UC-rich ssRNA and the corresponding ssDNA, dsRNA, and dsDNA were tested. The results showed that GST-tagged AtSKRP could interact with ssRNA but not the other types of nucleic acids (Figs 3a, S8b,c). In addition, both AG-rich and UC-rich ssRNA can be bound by AtSKRP (Fig. 3a), indicating a weak sequence preference of AtSKRP between the two tested sequences. Taken together, AtSKRP is able to bind ssRNA specifically *in vitro*.

AtSKRP is a bona fide RNA-binding protein that targets to 3' end of exon and intron of pre-mRNAs

Although AtSKRP has no known RNA-binding domains, the above results suggest AtSKRP may encode a bona fide RNA-binding protein. To test whether AtSKRP binds with RNA directly *in vivo*, we performed enhanced UV crosslinking and immunoprecipitation followed by sequencing (eCLIP-seq; Zhu *et al.*, 2020) using 35S:GFP-AtSKRP in *skrp* line. A 35S:GFP line was used as a negative control, and GFP-RZ-1C, a GFP tagged RNA-binding protein that previously characterized through eCLIP-seq, was used as a positive control (Zhu *et al.*, 2020) to monitor the eCLIP-seq workflow (Figs 3b, S8d). SKRP-eCLIP sequencing library was successfully constructed at a PCR cycle number similar to that for RZ-1C and much lower than that for GFP-only control (Fig. S8d), indicating SKRP indeed binds to RNA *in vivo*. Inspection of the sequencing data revealed good reproducibility between replicates as judged by the correlation of read counts (Fig. S8e). By using PIPE-CLIP, a tool for CLIP-seq

data analysis (Chen *et al.*, 2014), we identified 674 227 single-nucleotide crosslink sites that distributed at 8732 genes (Fig. S8f). Among these, 4448 genes display SKRP crosslink sites in all three biological repeats (Fig. S8f). These data suggest that AtSKRP directly binds to a broad range of RNAs *in vivo*.

Notably, c. 60% of these peaks are located at exons, while 21% are situated in introns (Fig. 3c), suggesting AtSKRP may directly bind with both mRNAs and pre-mRNAs. To further clarify the features of AtSKRP binding on different types of RNA, we assigned the eCLIP reads into different groups according to their location on mRNA (Fig. 3d). Most informatively, AtSKRP must be associated with an mRNA if a read is over the exon–exon junction. By contrast, AtSKRP must be associated with an unspliced pre-mRNA if a read is over an exon–intron junction or an intron–exon junction. Among all reads that can be aligned with introns and exons, 14.65% are located at exon–exon junctions, while 20.71% are located at exon–intron or intron–exon junctions (Fig. 3d), suggesting a stronger binding of SKRP toward unspliced pre-mRNAs compared with spliced RNAs. Importantly, given intronic region is much less abundant than the exon region at a steady state within the cell, SKRP binds, even more, stronger with unspliced pre-mRNA than spliced or mature mRNA, after normalization to the steady state input mRNA levels (Fig. 3e). Astonishingly, the alignment of crosslink sites that are derived from exon–intron junction reads revealed a sharp peak at –1 and –2 nt upstream of exon–intron junction (Fig. 3f). In addition, a peak c. –7 nt of an intron–exon junction can be also observed (Fig. 3f). Consistently, sequence features that underlie exon–intron boundary or intron–exon boundary such as GU and AG are highly enriched in sequences surrounding SKRP binding sites (Fig. 3g). No other obvious sequence feature was observed. This result suggests AtSKRP mainly targets RNA in a position-specific rather than sequence-



specific manner *in vivo*. In comparison, no obvious pattern was observed when the distribution of crosslink sites derived from exon–exon junction reads are examined (Fig. 3h). Taken together, these results suggest AtSKRP is a bona fide

RNA-binding protein that directly interacts with RNA *in vivo*. In addition, AtSKRP favors unspliced RNA over spliced RNA and specifically targets the 3' end of exons and introns at many pre-mRNAs (Fig. 3i).

Fig. 2 AtSKRP self-interact and forms oligomer *in vivo*, in association with its function in plant immunity. (a) Predictions of intrinsic disorder region of AtSKRP using PONDR. A PONDR score \geq or $<$ 0.5 corresponds to predicted disordered or ordered region, respectively. The ordered region (OR) is indicated by a gray box. The panel on top indicates the consensus sequence pattern of 18 SKRP homologous from different plant species. (b) OR deletion of AtSKRP attenuates its self-interaction in yeast. The schematic on top illustrates the construct used for this assay. The bottom shows the results from yeast two-hybrid assay. Yeast growth on SD/–Trp/–Leu (SD/–2) and SD/–Trp/–Leu/–His/–Ade (SD/–4) containing 5 mM 3-AT are both displayed. Growth on SD/–4 indicates interactions. Cells expressing GAL4-AD-T-antigen together with GAL4-BD-p53 or GAL4-BD-lamin C were used as positive and negative controls, respectively. (c) AtSKRP forms stable polymers *in vivo*. GFP-AtSKRP was immunoprecipitated from 35S:GFP-AtSKRP *atskrp-t* seedlings by using GFP antibody, followed by high salt treatment and then 5 min boiling in detergents (1% Triton X-100 and sodium deoxycholate) or denaturant 6 M urea, and subsequent 7 min boiling in the LDS loading buffer and DTT. Immunoblot analysis with anti-GFP antibody was performed. 35S:GFP was used as control. (d, e) The polymerization is partially impaired in GFP-AtSKRP^{ΔOR5} and GFP-AtSKRP^{ΔOR10}. GFP-AtSKRP^{ΔOR5} and GFP-AtSKRP^{ΔOR10} are expressed in *atskrp-t*, driven by 35S promoter. (d) Western blot results and (e) The results of band quantification by using IMAGEJ. Band 1, 2 indicates the dimmer and tetramer, while Bands 3–5 indicate the polymer of various forms of AtSKRP. 35S:GFP was used as control. (f) The biomass of *Phytophthora capsici* in infected Col-0, GFP-AtSKRP^{ΔOR5}, and GFP-AtSKRP^{ΔOR10}. Ten-day-old seedlings of Col-0 and various individual lines of GFP-AtSKRP^{ΔOR5} and GFP-AtSKRP^{ΔOR10} were infected by zoospores of *P. capsici*. GFP-AtSKRP was used as a positive control. The biomass was measured by using qPCR at 24 hpi. In DNA samples, ratios of *P. capsici* Actin over Arabidopsis *UBC9* were calculated and further normalized to such values in Col-0. Error bars indicate SD over three biological replicates. Asterisks indicate significant differences (***, $P < 0.001$).

AtSKRP associates with core spliceosome components PRP8 and BRR2 *in vivo*

Intriguingly, the specific RNA-binding pattern of AtSKRP at unspliced exon 3' end recapitulates that of yeast pre-mRNA processing factor 8 (Prp8), a core component of the U5 snRNP complex (Deng *et al.*, 2016; Chung *et al.*, 2019). We, therefore, hypothesized that AtSKRP might be associated with PRP8 and other spliceosome proteins. To test such a hypothesis, we analyzed the partners of AtSKRP through immunoprecipitation and mass spectrometry (IP-MS). Astonishingly, among various AtSKRP-associated proteins, PRP8 is among the top 10 proteins that showed the highest numbers of peptides in GFP-AtSKRP IP but not in GFP-only controls (Fig. 4a; Dataset S2). Various, other components of the spliceosome are also detected as potential partners of AtSKRP, such as components of tri-snRNP complex, BRR2 and GFA1; U2 snRNP auxiliary factors, U2AF35 and U2AF65; CDC5, a core subunit of the spliceosome-associated PRP nineteen complex (NTC); SR45, a plant-specific SR protein and component of spliceosome-associated ASAP complex (Palma *et al.*, 2007; Shi, 2017; Fig. 4a; Dataset S2). These interactions captured *in vivo* were further tested in yeast by using a Y2H assay. In consistent with the IP-MS results, AtSKRP also interacts with CDC5, U2AF65a, and SR45 in yeast (Fig. 4b). The Y2H test toward PRP8 and BRR2 was not successful, due to the failure of expression of these large proteins in yeast (Figs 4b, S9), in consistent with previous reports (van Nues & Beggs, 2001; Liu *et al.*, 2006). As negative control, depletion of C terminus of AtSKRP disrupt its interaction with CDC5 and SR45 in yeast (Fig. 4c). In the meanwhile, the *in vivo* interactions between AtSKRP and PRP8 or BRR2 are confirmed through Co-IP assays by using GFP-AtSKRP transgenic line and anti-PRP8 or anti-BRR2 antibody (Fig. 4d). We further tested whether these interaction partners of AtSKRP also participate in plant immunity. Upon *P. capsici* infection, we found loss of PRP8 decreases plant immunity while loss of SR45 increases plant immunity. In comparison, loss of U2AF65a or CDC5 does not affect plant immunity (Fig. S10). Thus, consistent with the observed association with AtSKRP, PRP8, and SR45 also

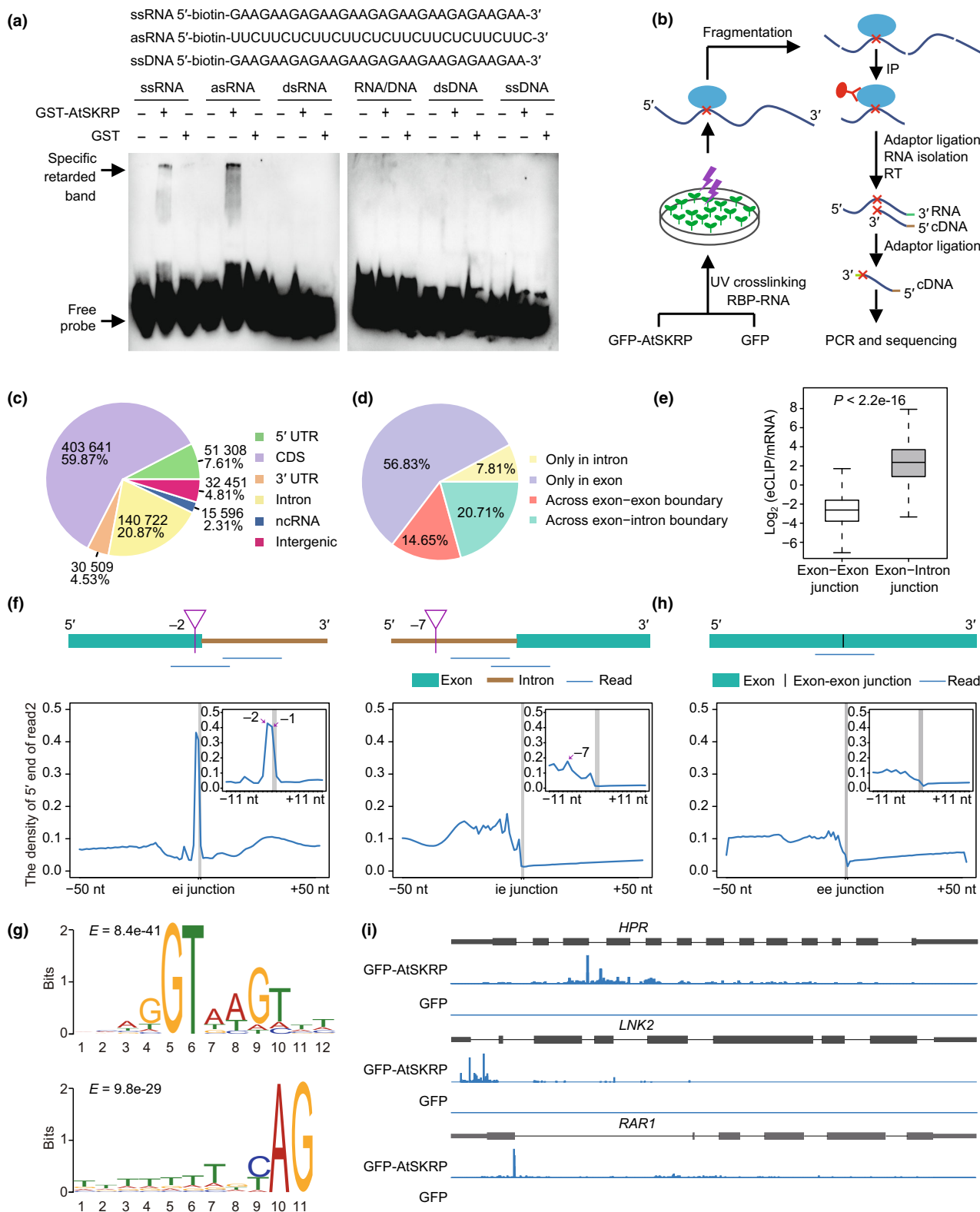
participate in plant immunity. In addition, SKRP likely antagonizes the function or modulates the activity of PRP8 (see the Discussion section).

AtSKRP regulates pre-mRNAs splicing in connection with its RNA-binding

The above results suggested that AtSKRP is associated with spliceosome and unspliced pre-mRNA. Thus, we tested whether AtSKRP regulates pre-mRNA splicing and wondered the potential connection between its RNA-binding and splicing regulation. We performed mRNA-Seq in *atskrp-t* and Col-0 infected by *P. capsici* at 0 and 24 hpi. Next, to measure altered splicing upon loss of SRKP, we calculated the ratio of an intron relative to the adjacent exons and identified cases where such a ratio is significantly different between Col-0 and *atskrp-t* (see the Materials and Methods section). In total, 113 and 122 differential splicing events corresponding to 100 and 103 genes were identified in *atskrp-t* compared with Col-0 at 0 and 24 hpi, respectively (Fig. 5a; Dataset S3). At 0 hpi, there are 54 and 59 introns being removed more and less effectively being removed more and less effectively in *atskrp-t*, respectively (Fig. 5a; Dataset S3). Therefore, AtSKRP may play both positive and negative roles in splicing at distinct introns. Notably, c. 80% of the genes containing SKRP-regulated splicing events are bound by SKRP in our eCLIP data (Fig. 5b). In comparison, only 30% of the expressed genes without SKRP-regulated splicing events are bound by SRKP (Fig. 5b). The differential splicing events, as well as the SKRP's RNA-binding at selected genes, are further confirmed through RT-qPCR and RIP-qPCR, respectively (Fig. 5c,d, also see paragraph below). Taken together, we conclude AtSKRP regulates pre-mRNA splicing in association with its direct RNA binding.

AtSKRP represses intron removal at a few genes that promote susceptibility to *P. capsici*

Next, we explore the link between SKRP-regulated splicing and the increased susceptibility to *P. capsici* upon loss of SKRP. Among genes containing differential splicing events that are



detected in *atskrp-t*, there are only a few genes related to plant immunity by annotation (Dataset S3). At 0 hpi, there are 11 and 5 positive immunity regulators containing exons that are spliced more and less effectively in *atskrp-t*, while there are four and four negative immunity regulators containing exons that are spliced

more and less effectively in *atskrp-t* (Fig. 5a; Dataset S3). At 24 hpi, there are nine and seven positive immunity regulators containing exons that are spliced more and less effectively in *atskrp-t*, while there are one and one negative immunity regulators containing exons that are spliced more and less effectively in

Fig. 3 SKRP targets to unspliced exon 3' end as revealed by eCLIP-seq. (a) Gel shift results show that AtSKRP binds single-stranded RNA specifically *in vitro*. Photograph shows the signals generated from biotin-labelled probes. *In vitro* purified GST-AtSKRP or GST alone was used in the assay. Different types of nucleic acids were tested; ssRNA, sense single-stranded RNA; asRNA, antisense single-stranded RNA that is complementary to ssRNA; ssDNA, sense single-stranded DNA; dsDNA, double-strand DNA; RNA/DNA, RNA/DNA hybrid of ssDNA and asRNA. (b) A cartoon illustrates a brief workflow and the principle of AtSKRP-eCLIP-seq (For details, see the [Materials and Methods](#) section). Blue circles indicate SKRP; dark-blue solid lines indicate RNAs; dark-blue dashed lines indicate fragmented RNAs; red crosses indicate cross-link sites. (c) Pie chart showing the distribution of eCLIP xlsites (significant crosslinked sites) at exons, introns, 5' UTRs, 3' UTRs, ncRNAs, and intergenic region. The percentage of sites and the number of sites in each category are shown. (d) Distribution of eCLIP reads that are mapped to generic regions. The percentage of reads in each category is shown. (e) Box plots demonstrate the relative binding strength of AtSKRP at spliced and unspliced RNAs. At each exon-exon or exon-intron junction, the reads density of eCLIP reads spanning such junction was normalized to the read density in mRNA-Seq. The box plot shows the median and 25th and 75th percentiles with whiskers extending to 1.5 times of the interquartile range from the 25th and 75th percentiles. (f) Distribution of GFP-AtSKRP-eCLIP xlsites (blue lines) along exon-intron and intron-exon units. The position of PRP8 in yeast is marked by purple triangles. The inset area displays the same data within a narrower window on the X-axis. (g) Motifs that enriched around GFP-AtSKRP-eCLIP xlsites at exon-intron junction (top) and intron-exon junction (bottom). ± 10 bp surround eCLIP xlsites were used for MEME-ChIP analysis. (h) Distribution of GFP-AtSKRP-eCLIP xlsites over exon-exon junction. The inset area displays the same data within a narrower window on the X-axis. (i) Genome browser view of AtSKRP-binding sites on three individual genes.

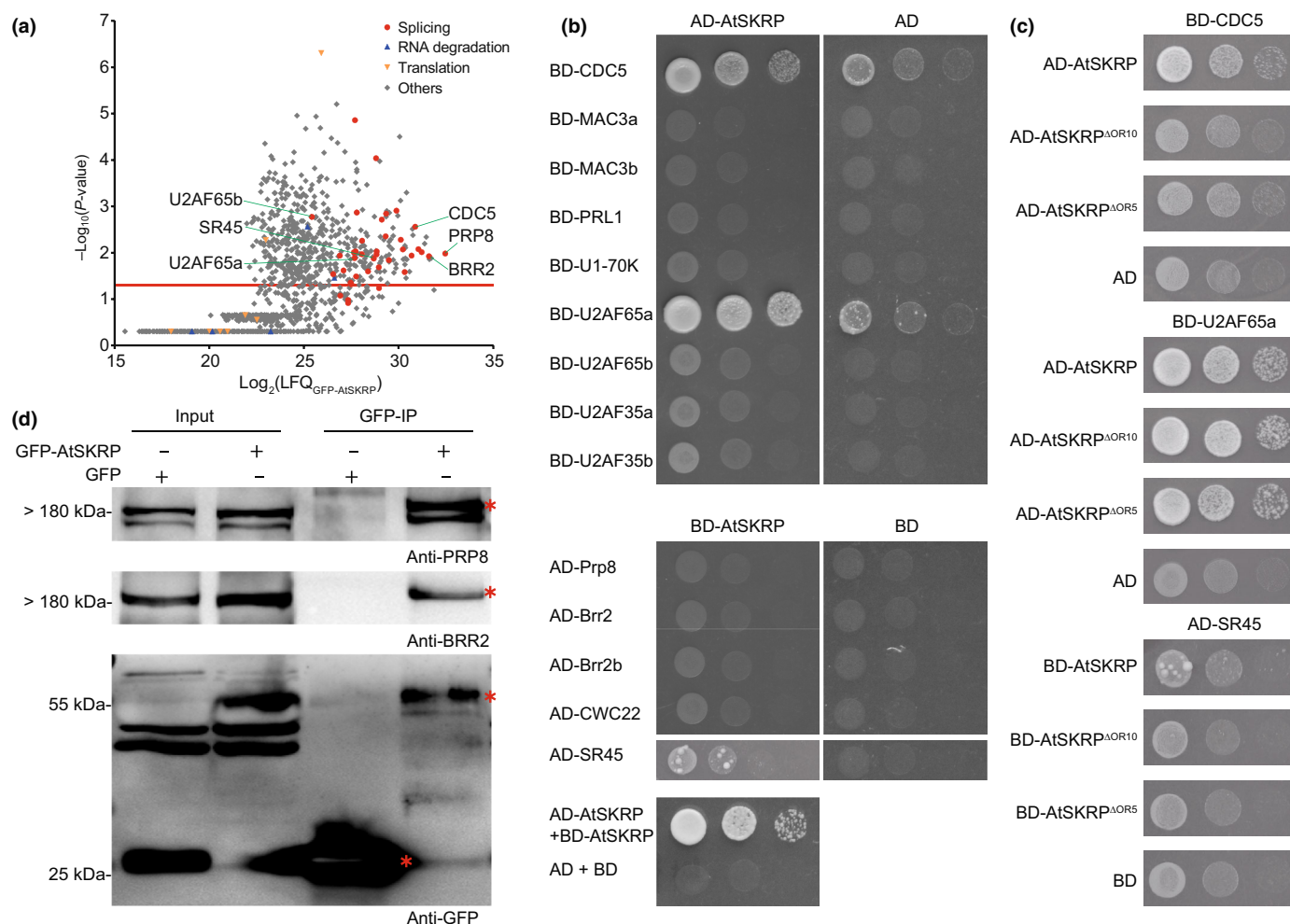
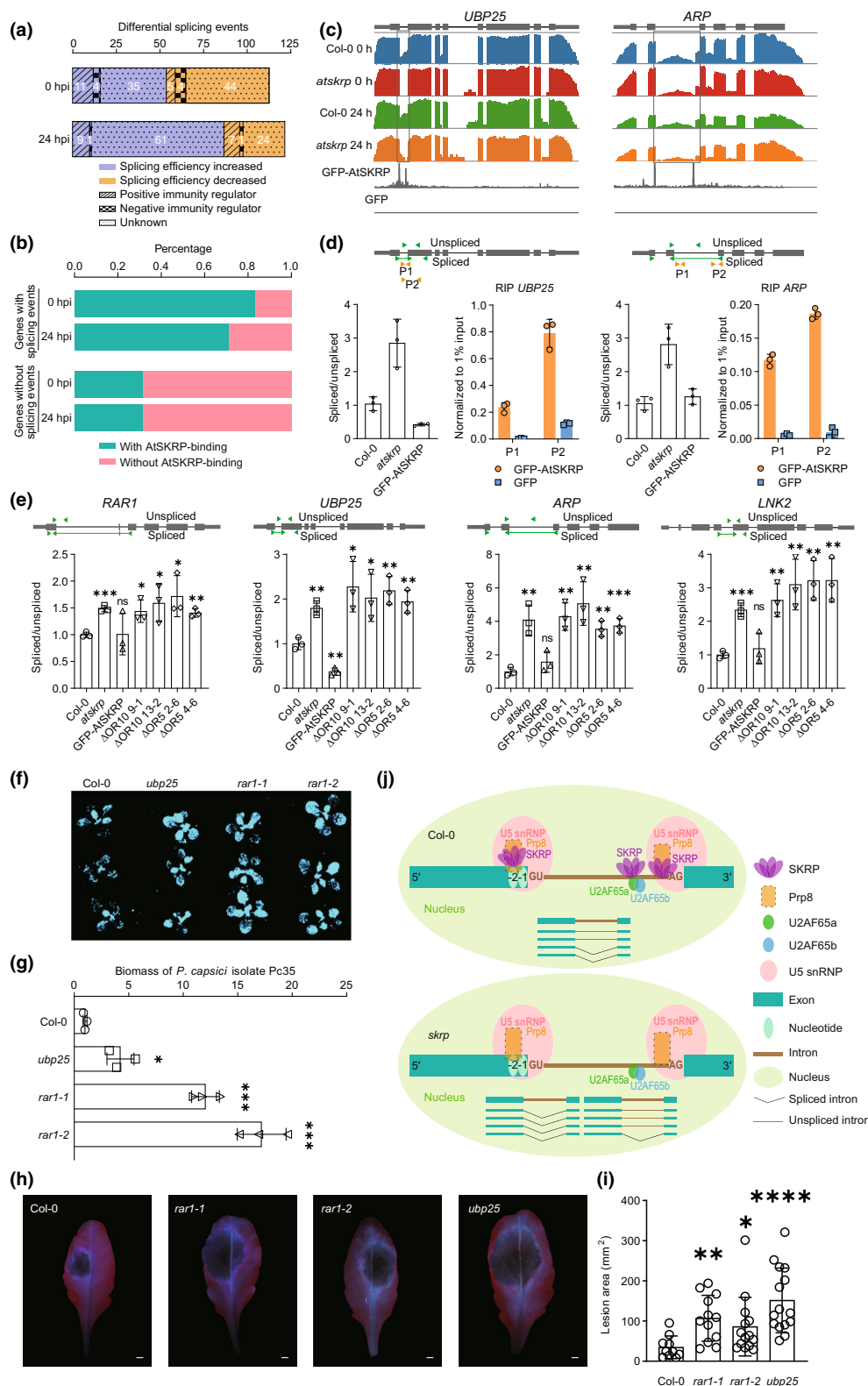


Fig. 4 AtSKRP associates with core spliceosome proteins PRP8 and BRR2. (a) IP-MS results for GFP-AtSKRP. Scatter plot indicates proteins specifically associated with GFP-AtSKRP compared with the 35S:GFP control. Proteins belonging to different functional groups are highlighted. Various spliceosome proteins were detected. *P*-values were calculated based on LFQ (label-free quantitation) values between GFP-AtSKRP and GFP alone. (b) AtSKRP interacts with SR45, U2AF65a, and CDC5 as revealed by yeast two-hybrid assay. (c) Co-IP results demonstrate *in vivo* association of AtSKRP with PRP8 and BRR2. PRP8 and BRR2 were detected by using anti-PRP8 and anti-BRR2 antibody. (d) OR deletion of AtSKRP attenuates the interaction with CDC5 and SR45 in yeast. SD/-Trp/-Leu/-His/-Ade (SD/-4) are displayed. Red asterisk indicates the position of target band.

atskrp-t (Fig. 5a; Dataset S3). Overall, there are in general more positive immunity regulators than negative immunity regulators being regulated by SKRP in terms of pre-mRNA splicing. In addition, for immunity regulators, the increased splicing

efficiency is more frequently observed than the decreased splicing efficiency, upon loss of SKRP.

In consistent with the general trend as stated above, SKRP represses the intron splicing of *Required for Mla12 Resistance 1*



(RAR1), a positive regulator of plant immunity (Shirasu *et al.*, 1999; Azevedo *et al.*, 2002; Muskett *et al.*, 2002; Tornero *et al.*, 2002; Takahashi *et al.*, 2003; Thao *et al.*, 2007; Zhang *et al.*, 2010). We further hypothesized that SKRP might negatively impact plant immunity by repressing splicing of positive

regulators of immunity like RAR1. To test this hypothesis, we selected another three genes *Ubiquitin-Specific Protease 25* (*UBP25*), *Ankyrin Repeat Protein* (*ARP*), and *Night Light-inducible and Clock-regulated Gene 2* (*LNK2*), in addition to *RAR1* for further analysis. In consistent with the RNA-Seq data,

Fig. 5 AtSKRP suppresses pre-mRNA splicing of a few positive immunity regulators. (a) A summary of differentially splicing events in *atskrp* compared with Col-0 as detected by mRNA-Seq. The numbers above the bar indicate the numbers of differential splicing events. The numbers within the bar indicate the numbers of genes that display increased or decreased splicing events in *atskrp* vs Col-0. Numbers of annotated positive or negative immunity regulators with differential splicing events are also indicated. (b) A bar chart displays ratios of genes with or without AtSKRP binding in gene groups with or without differential splicing events in *atskrp* vs Col-0. (c, d) Example genes that are bound by AtSKRP (as identified by AtSKRP-eCLIP-seq) and differentially spliced in *atskrp* vs Col-0. (c) Sequencing results of mRNA-Seq, GFP-AtSKRP-eCLIP-seq, and GFP-eCLIP-seq are shown in different panels, and affected introns are indicated with gray boxes. (d) RT-qPCR validation of altered splicing efficiency and RIP-qPCR validation of AtSKRP RNA binding. Splicing efficiency was measured as the ratio of spliced over unspliced RNA levels. Primer locations are indicated at the top panel. RIP data are presented as IP/% input. Values present mean \pm SD over three biological replicates. (e) AtSKRP suppresses intron splicing on four selected genes, depending on its ordered region (OR) at C terminus. Splicing efficiency was measured as ratio of spliced over unspliced RNA levels and presented as mean \pm SD over three biological replicates. (f) *ubp25*, *rar1-1*, and *rar1-2* showed more susceptibility to *Phytophthora capsici* isolate Pc35-Luc infection compared with Col-0. The image was taken at 12 hpi. (g) The biomass of Pc35-Luc in infected Col-0, *ubp25*, *rar1-1*, and *rar1-2*. Ten-day-old seedlings of Col-0, *ubp25*, *rar1-1*, and *rar1-2* were infected by zoospores of Pc35-Luc. The biomass was measured the same way as in Fig. 1(e). Values present mean \pm SD over three biological replicates. (h) *rar1-1*, *rar1-2*, and *ubp25* showed more susceptibility to *P. capsici* in 4-wk-old seedlings. Photographs were taken at 48 hpi under UV light. Bar, 2 mm. (i) Lesion area of infected leaves in (h). Lesion areas were measured at 48 hpi. Means and SD from separate measurements are shown (*, $P < 0.05$; **, $P < 0.01$; ****, $P < 0.0001$). (j) A proposed working model for the role of AtSKRP in regulating pre-mRNA splicing. SKRP associates with U5 snRNP components such as PRP8 and BRR2 to target exon and intron 3' end before splicing occurs. Loss of SKRP results in both increased and decreased splicing efficiency in different cases. This includes increased splicing efficiency at several positive immunity regulators.

all four genes showed increased intron removal efficiency in *atskrp* (Fig. 5e), indicating SKRP represses the splicing of certain exons at these genes. In addition, all four genes are direct targets of SKRP as judged by SKRP-eCLIP-seq and RIP-qPCR data (Figs 5c,d, S11). Notably, in addition to *atskrp*, the increased intron removal efficiency compared with Col-0 was also observed in dominant negative *skrp* mutants GFP-AtSKRP^{ΔOR10} and GFP-AtSKRP^{ΔOR5} (Fig. 5e). Thus, the disrupted polymerization activity as observed in these mutants likely also contributes to SKRP's function in splicing repression of these genes. Next, we checked whether UBP25, ARP, LNK2, and RAR1 are functionally important for plant immunity against *P. capsici*. Transient assay in *N. benthamiana* leaf showed overexpression of UBP25 and RAR1 but not of LNK2 and ARP, conferred increased resistance against *P. capsici* (Fig. S12). Consistently, T-DNA insertion mutants *ubp25*, *rar1-1*, and *rar1-2* showed more susceptibility compared with wild-type Col-0 (Figs 5f,g, S13a,b), indicating that UBP25 and RAR1 positively regulate plant immunity against *P. capsici* in Arabidopsis.

In contrast to *atskrp*, we found that the intron removal efficiency of UBP25 was decreased in *prp8*, indicating SKRP may antagonize PRP8 also in terms of UBP25 splicing (Fig. S14a). In addition, the intron removal efficiency of both UBP25 and RAR1 was similarly increased in *atskrp*, *sr45*, and *sr45 atskrp* double mutant compared with Col-0, indicating SKRP function in a same genetic pathway as SR45 in repressing pre-mRNA splicing (Fig. S14b). These data further strength that the interactions observed between SKRP and PRP8 or SR45 is functionally relevant to the pre-mRNA splicing regulated by SKRP.

Next, we further checked whether the enhanced splicing efficiency of UBP25 and RAR1 in *atskrp* impact plant immunity. As shown by both RNA-Seq data and qPCR quantification, we found that the loss of AtSKRP does not influence the level of spliced UBP25 and RAR1 but decrease the level of the unspliced transcripts (Figs 5c, S10, S15a). Thus, we hypothesize that the presence of unspliced transcripts could somehow interfere the spliced transcripts. To test such hypothesis, we expressed the spliced transcripts of UBP25 and RAR1 transiently in

N. benthamiana leaves and compared the plant immunity upon *P. capsici* infection with or without co-expressing the corresponding unspliced transcripts. Intriguingly, the presence of unspliced transcript indeed reduces plant immunity against *P. capsici* (Fig. S15b–d). In the meantime, neither the RNA nor the protein expression levels corresponding to the spliced transcripts was affected by the expression of the unspliced transcript (Fig. S15e–h). Importantly, the unspliced transcript can be translated into a truncated protein due to the presence of premature stop codon within the retained intron (Fig. S15f,h). Thus, our data indicate that by encoding a truncated protein, the presence of unspliced transcript of UBP25 and RAR1 interferes with the function of their corresponding full-length protein that encoded by fully spliced transcript. Taken together, our mechanistic study reveals that AtSKRP, a novel spliceosome-associated protein, targets exon 3' end of unspliced RNA and represses intron removal at positive immune regulatory genes to repress plant immunity (Fig. 5h).

Discussion

In this study, we investigated the molecular function of SKRP in Arabidopsis. Like its ortholog in soybean, loss of AtSKRP leads to increased plant immunity to *P. capsici*. AtSKRP forms polymers both *in vitro* and *in vivo*, an activity that is in part regulated by its C-terminus monkey tail-like domain. Most strikingly, AtSKRP represents a bona fide RNA-binding protein that is directly and specifically targeted to exon 3' end of unspliced pre-mRNAs. Consistently, AtSKRP associates with core components of spliceosome such as BRR2 and PRP8, which showed a similar RNA-binding pattern as SKRP in yeast. Finally, in association with its RNA-binding, AtSKRP regulates the splicing of more than a hundred genes including a few disease-related genes. Specifically, AtSKRP binds the unspliced RNA and represses intron splicing of UBP25 and RAR1, both of which are the positive regulators of plant immunity.

The exact protein domain responsible for the RNA-binding of SKRP remains elusive, as there is no known RNA-binding

domain. Given the majority of SKRP are intrinsically disordered sequences, the RNA binding of SKRP could be attributed to the positively charged amino acids within this region. Indeed, RNA-binding proteins are enriched for intrinsically disordered regions that could contribute to RNA-binding. In addition, the polymerization, the immunity suppression activity, and also the splicing suppression of SKRP are disrupted when the C-terminus monkey tail-like region is depleted, indicating C terminus of SKRP is critical for its function, potentially including its faithful RNA-binding, a hypothesis remains to be further elucidated. The fact that SKRP binds RNA directly in a position-specific manner is also intriguing. No other sequence features were observed around SKRP binding sites, except for the conserved intron end sequences GU and AG (Fig. 3g). Therefore, it is most likely that SKRP is targeted to the exon 3' end and intron 3' end of unspliced RNA together with the spliceosome. Consistently, we did not observe RNA sequence preference of SKRP *in vitro*, as it binds both GA-rich and CU-rich sequences at similar strength. Of note, although SKRP favors exon and intron 3' end of unspliced RNA, the RNA-binding outside these optimal positions can be observed (e.g. Fig. 3i). Therefore, some sequence preference regarding to SKRP RNA-binding cannot be excluded.

The exact mode of action of SKRP in splicing regulation is partially elucidated in the current study. The spliceosome assembly initiates from E complex formation (Shi, 2017). U2AF⁶⁵ binds to the polypyrimidine (Py) tract and simultaneously, SF1 binds to the BS (Berglund *et al.*, 1998; Selenko *et al.*, 2003). This cooperation is critical for initial BS recognition and the stabilization of the E complex (Berglund *et al.*, 1998; Selenko *et al.*, 2003). The pre-mRNA splicing consists of two steps of transesterification, known as branching and exon ligation (Shi, 2017). During the two steps, Prp8-mRNA interaction switches from the 5' splice site (5'SS) and the branch site (BS) to the 3' splice site (3'SS; Chung *et al.*, 2019). It has been reported that U2AF^{65a/b} interacts with SF1 in Arabidopsis (Jang *et al.*, 2014), which is similar to the previous results in humans. We found that AtSKRP interacts with U2AF65a in yeast and associates with PRP8 *in vivo*. Furthermore, SKRP binds the 3' end of the unspliced exon around the 5'SS and 3' end of the intron, which is similar to Prp8 and U2AF65 (Shi, 2017; Chung *et al.*, 2019). These data indicate that AtSKRP may be engaged during the entire pre-mRNA splicing cycle. How SKRP could behave as both positive and negative regulator of splicing at different genes remains to be further explored in the future. The majority of SKRP protein sequence are intrinsic disordered; thus, SKRP may be involved in lots of transient and weak interactions *in vivo*, which may contribute to its splicing inhibition or promotion at different set of genes. Consistently, our data indicate SKRP likely antagonizes the function of PRP8 while facilitates the function of SR45 at its targets such as *UBP25* (Figs S10, S14). In summary, SKRP is likely a peripheral factor of spliceosome thus modulates splicing in a context-dependent manner.

How exactly SKRP regulates plant immunity in connection with its RNA-binding and splicing regulation remains to be further explored in the future. Current data showed SKRP suppresses the intron splicing of a few positive regulators of plant

immunity. Whether such action is sufficient to confer the immunity suppression function of SKRP remains to be tested more rigorously. Notably, the possibility of SKRP in regulating other aspects of RNA metabolism in addition to splicing cannot be ruled out at the moment. Interestingly, various other regulators of plant immunity were also recovered as potential partners of SKRP in our IP-MS assay, including CDC5, PRL1, MAC3A, MAC3B, and SE (Palma *et al.*, 2007; Monaghan *et al.*, 2009; Niu *et al.*, 2016; Dataset S2). Intriguingly, these proteins were shown to regulate pre-mRNA splicing as well as miRNA biogenesis (Zhang *et al.*, 2013, 2014; Raczyńska *et al.*, 2014; Li *et al.*, 2018), a potential aspect that is worth testing for SKRP in the future. Nevertheless, we showed SKRP encodes a spliceosome-associated RNA-binding protein that directly targets exon 3' end to regulate splicing; this result provides evidence that plant immunity regulators such as SKRP can have a direct association with the core spliceosome.

Our studies demonstrated that SKRP is a negative regulator of immunity against *Phytophthora* in both Soybean and Arabidopsis. *RARI*, one of the SKRP downstream-regulated genes, functions in R gene-dependent immunity in Arabidopsis and Barley against different pathogens in a quantitative manner (Shirasu *et al.*, 1999; Muskett *et al.*, 2002; Tornero *et al.*, 2002). This information encourages us to test whether editing of SKRP confers broad resistance to different plant pathogens. Given SKRP orthologs are prevalent in a wide range of plant species including important crops and the SKRP mutants do not illustrate visible growth penalty in our assays, SKRP could be served as a novel gene-editing target to improve crop disease-resistant trait.

Acknowledgements

We thank Dr Xiaofeng Cao (Chinese Academy of Sciences) for providing anti-PRP8 and anti-BRR2 antibodies; Dr Xin Gong, Dr Sisi Li, and Dr Fan Zou (Southern University of Science and Technology) for help on gel filtration; Dr Fei Mao (Nanjing Agricultural University) for help on eCLIP-seq data analysis; Dr Paul R.J. Birch (University of Dundee) for providing BiFC vectors pCL112 and pCL113; Dr Xinjian He (National Institute of Biological Sciences) for providing *cdc5-1* and Dr A.S.N. Reddy (Colorado State University) for providing *sr45* mutant; and Dr Han Chen (Nanjing Agricultural University) for providing *P. capsici* isolate Pc35-Luc. We thank all the members from Wu and Dong Lab for discussion. This work was supported by the National Natural Science Foundation of China (31970277 and 32170348 to ZW; 32130088 and 31721004 to SD), Guangdong Innovation Research Team fund (2016ZT06S172), Shenzhen Innovation Committee of Science and Technology (JCYJ20190809141201671 to DZ and KYTDPT20181011104005 to ZW), and Key Laboratory of Molecular Design for Plant Cell Factory of Guangdong Higher Education Institutes (2019KSYS006).





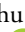



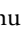
Competing interests

None declared.

Author contributions

ZW and SD conceived and supervised the study. LC, JH and DZ performed experiments. ZX, HS, YH and YW performed bioinformatic analysis. LC, SD and ZW wrote the paper with input from all authors.

ORCID

Ling Chen  <https://orcid.org/0000-0001-8711-047X>
 Suomeng Dong  <https://orcid.org/0000-0002-9623-6776>
 Jie Huang  <https://orcid.org/0000-0002-6657-8740>
 Yufan Hui  <https://orcid.org/0000-0002-1581-2090>
 Haidong Shu  <https://orcid.org/0000-0002-9769-8278>
 Yufeng Wu  <https://orcid.org/0000-0002-9086-6080>
 Zhe Wu  <https://orcid.org/0000-0001-9436-3299>
 Zhihui Xu  <https://orcid.org/0000-0001-5698-8175>
 Danling Zhu  <https://orcid.org/0000-0003-3385-403X>

Data availability

The raw sequence data reported in this paper have been deposited in the Genome Sequence Archive (Chen *et al.*, 2021) in National Genomics Data Center (CNCB-NGDC Members and Partners, 2023), China National Center for Bioinformation/Beijing Institute of Genomics, and Chinese Academy of Sciences (GSA: CRA006308) that are publicly accessible at <https://ngdc.cncb.ac.cn/gsa>.

References

- Ali GS, Palusa SG, Golovkin M, Prasad J, Manley JL, Reddy AS. 2007. Regulation of plant developmental processes by a novel splicing factor. *PLoS ONE* 2: e471.
- Anders S, Pyl PT, Huber W. 2015. HTSeq – a PYTHON framework to work with high-throughput sequencing data. *Bioinformatics* 31: 166–169.
- Azevedo C, Sadanandom A, Kitagawa K, Freialdenhoven A, Shirasu K, Schulze-Lefert P. 2002. The RAR1 interactor SGT1, an essential component of R gene-triggered disease resistance. *Science* 295: 2073–2076.
- Barta A, Kalyna M, Reddy AS. 2010. Implementing a rational and consistent nomenclature for serine/arginine-rich protein splicing factors (SR proteins) in plants. *Plant Cell* 22: 2926–2929.
- Bentley DL. 2014. Coupling mRNA processing with transcription in time and space. *Nature Reviews Genetics* 15: 163–175.
- Berglund JA, Abovich N, Rosbash M. 1998. A cooperative interaction between U2AF65 and mBBP/SF1 facilitates branchpoint region recognition. *Genes & Development* 12: 858–867.
- Bessonov S, Anokhina M, Will CL, Urlaub H, Luhrmann R. 2008. Isolation of an active step I spliceosome and composition of its RNP core. *Nature* 452: 846–850.
- Bjornson M, Pimprikar P, Nurnberger T, Zipfel C. 2021. The transcriptional landscape of *Arabidopsis thaliana* pattern-triggered immunity. *Nature Plants* 7: 579–586.
- Chen B, Yun J, Kim MS, Mendell JT, Xie Y. 2014. PIPE-CLIP: a comprehensive online tool for CLIP-seq data analysis. *Genome Biology* 15: R18.
- Chen H, Zou Y, Shang Y, Lin H, Wang Y, Cai R, Tang X, Zhou JM. 2008. Firefly luciferase complementation imaging assay for protein–protein interactions in plants. *Plant Physiology* 146: 368–376.
- Chen T, Chen X, Zhang S, Zhu J, Tang B, Wang A, Dong L, Zhang Z, Yu C, Sun Y *et al.* 2021. The genome sequence archive family: toward explosive data growth and diverse data types. *Genomics, Proteomics & Bioinformatics* 19: 578–583.
- Cheng YT, Germain H, Wiermer M, Bi DL, Xu F, Garcia AV, Wirthmueller L, Despres C, Parker JE, Zhang YL *et al.* 2009. Nuclear pore complex component MOS7/Nup88 is required for innate immunity and nuclear accumulation of defense regulators in *Arabidopsis*. *Plant Cell* 21: 2503–2516.
- Chung CS, Tseng CK, Lai YH, Wang HF, Newman AJ, Cheng SC. 2019. Dynamic protein–RNA interactions in mediating splicing catalysis. *Nucleic Acids Research* 47: 899–910.
- Clough SJ, Bent AF. 1998. Floral dip: a simplified method for *Agrobacterium*-mediated transformation of *Arabidopsis thaliana*. *The Plant Journal* 16: 735–743.
- CNCB-NGDC Members and Partners. 2023. Database resources of the National Genomics Data Center, China National Center for Bioinformation in 2023. *Nucleic Acids Research* 51: D18–D28.
- Couto D, Zipfel C. 2016. Regulation of pattern recognition receptor signalling in plants. *Nature Reviews Immunology* 16: 537–552.
- Cui H, Tsuda K, Parker JE. 2015. Effector-triggered immunity: from pathogen perception to robust defense. *Annual Review of Plant Biology* 66: 487–511.
- Deng X, Gu L, Liu C, Lu T, Lu F, Lu Z, Cui P, Pei Y, Wang B, Hu S *et al.* 2010. Arginine methylation mediated by the *Arabidopsis* homolog of PRMT5 is essential for proper pre-mRNA splicing. *Proceedings of the National Academy of Sciences, USA* 107: 19114–19119.
- Deng X, Lu T, Wang L, Gu L, Sun J, Kong X, Liu C, Cao X. 2016. Recruitment of the NineTeen complex to the activated spliceosome requires AtPRMT5. *Proceedings of the National Academy of Sciences, USA* 113: 5447–5452.
- Dinesh-Kumar SP, Baker BJ. 2000. Alternatively spliced N resistance gene transcripts: their possible role in tobacco mosaic virus resistance. *Proceedings of the National Academy of Sciences, USA* 97: 1908–1913.
- Garland W, Jensen TH. 2020. Nuclear sorting of RNA. *Wiley Interdisciplinary Reviews: RNA* 11: e1572.
- Germain H, Qu N, Cheng YT, Lee E, Huang Y, Dong OX, Gannon P, Huang S, Ding P, Li Y *et al.* 2010. MOS11: a new component in the mRNA export pathway. *PLoS Genetics* 6: e1001250.
- Goritschnig S, Weihmann T, Zhang Y, Fobert P, McCourt P, Li X. 2008. A novel role for protein farnesylation in plant innate immunity. *Plant Physiology* 148: 348–357.
- Goritschnig S, Zhang YL, Li X. 2007. The ubiquitin pathway is required for innate immunity in *Arabidopsis*. *The Plant Journal* 49: 540–551.
- Howard BE, Hu Q, Babaoglu AC, Chandra M, Borghi M, Tan X, He L, Winter-Sederoff H, Gassmann W, Veronese P *et al.* 2013. High-throughput RNA sequencing of pseudomonas-infected *Arabidopsis* reveals hidden transcriptome complexity and novel splice variants. *PLoS ONE* 8: e74183.
- Huang J, Gu L, Zhang Y, Yan T, Kong G, Kong L, Guo B, Qiu M, Wang Y, Jing M *et al.* 2017. An oomycete plant pathogen reprograms host pre-mRNA splicing to subvert immunity. *Nature Communications* 8: 2051.
- Huang J, Lu X, Wu H, Xie Y, Peng Q, Gu L, Wu J, Wang Y, Reddy ASN, Dong S. 2020. Phytophthora effectors modulate genome-wide alternative splicing of host mRNAs to reprogram plant immunity. *Molecular Plant* 13: 1470–1484.
- Huppertz I, Attig J, D'Ambrogio A, Easton LE, Sibley CR, Sugimoto Y, Tajnik M, König J, Ule J. 2014. iCLIP: protein–RNA interactions at nucleotide resolution. *Methods* 65: 274–287.
- Jang YH, Park HY, Lee KC, Thu MP, Kim SK, Suh MC, Kang H, Kim JK. 2014. A homolog of splicing factor SF1 is essential for development and is involved in the alternative splicing of pre-mRNA in *Arabidopsis thaliana*. *The Plant Journal* 78: 591–603.
- Jones JD, Dangl JL. 2006. The plant immune system. *Nature* 444: 323–329.
- Jurica MS, Moore MJ. 2003. Pre-mRNA splicing: awash in a sea of proteins. *Molecular Cell* 12: 5–14.
- Kalyna M, Simpson CG, Syed NH, Lewandowska D, Marquez Y, Kusenda B, Marshall J, Fuller J, Cardle L, McNicol J *et al.* 2012. Alternative splicing and nonsense-mediated decay modulate expression of important regulatory genes in *Arabidopsis*. *Nucleic Acids Research* 40: 2454–2469.
- Kastner B, Will CL, Stark H, Luhrmann R. 2019. Structural insights into nuclear pre-mRNA splicing in higher eukaryotes. *Cold Spring Harbor Perspectives in Biology* 11: a032417.
- Kim D, Paggi JM, Park C, Bennett C, Salzberg SL. 2019. Graph-based genome alignment and genotyping with HISAT2 and HISAT-genotype. *Nature Biotechnology* 37: 907–915.

- Kong L, Feng B, Yan Y, Zhang C, Kim JH, Xu L, Rack JGM, Wang Y, Jang JC, Ahel I *et al.* 2021. Noncanonical mono(ADP-ribosyl)ation of zinc finger SZF proteins counteracts ubiquitination for protein homeostasis in plant immunity. *Molecular Cell* 81: 4591–4604.
- Lee WC, Hou BH, Hou CY, Tsao SM, Kao P, Chen HM. 2020. Widespread exon junction complex footprints in the RNA degradome mark mRNA degradation before steady state translation. *Plant Cell* 32: 904–922.
- Li S, Liu K, Zhou B, Li M, Zhang S, Zeng L, Zhang C, Yu B. 2018. MAC3A and MAC3B, two core subunits of the MOS4-associated complex, positively influence miRNA biogenesis. *Plant Cell* 30: 481–494.
- Li S, Wang Y, Zhao Y, Zhao X, Chen X, Gong Z. 2020. Global co-transcriptional splicing in Arabidopsis and the correlation with splicing regulation in mature RNAs. *Molecular Plant* 13: 266–277.
- Li X, Clarke JD, Zhang Y, Dong X. 2001. Activation of an EDS1-mediated R-gene pathway in the *snc1* mutant leads to constitutive, NPR1-independent pathogen resistance. *Molecular Plant–Microbe Interactions* 14: 1131–1139.
- Li Y, Tessaro MJ, Li X, Zhang Y. 2010. Regulation of the expression of plant resistance gene SNC1 by a protein with a conserved BAT2 domain. *Plant Physiology* 153: 1425–1434.
- Liu S, Rauhut R, Vornlocher HP, Luhrmann R. 2006. The network of protein–protein interactions within the human U4/U6.U5 tri-snRNP. *RNA* 12: 1418–1430.
- Machanic P, Bailey TL. 2011. MEME-CHIP: motif analysis of large DNA datasets. *Bioinformatics* 27: 1696–1697.
- Mandadi KK, Scholthof KB. 2015. Genome-wide analysis of alternative splicing landscapes modulated during plant–virus interactions in *Brachypodium distachyon*. *Plant Cell* 27: 71–85.
- Marquardt S, Raitskin O, Wu Z, Liu F, Sun Q, Dean C. 2014. Functional consequences of splicing of the antisense transcript COOLAIR on FLC transcription. *Molecular Cell* 54: 156–165.
- Marquez Y, Brown JW, Simpson C, Barta A, Kalyna M. 2012. Transcriptome survey reveals increased complexity of the alternative splicing landscape in Arabidopsis. *Genome Research* 22: 1184–1195.
- Marquez Y, Hopfner M, Ayatollahi Z, Barta A, Kalyna M. 2015. Unmasking alternative splicing inside protein-coding exons defines exons and their role in proteome plasticity. *Genome Research* 25: 995–1007.
- Meyer K, Koster T, Nolte C, Weinholdt C, Lewinski M, Grosse I, Staiger D. 2017. Adaptation of iCLIP to plants determines the binding landscape of the clock-regulated RNA-binding protein AtGRP7. *Genome Biology* 18: 204.
- Monaghan J, Xu F, Gao M, Zhao Q, Palma K, Long C, Chen S, Zhang Y, Li X. 2009. Two Prp19-like U-box proteins in the MOS4-associated complex play redundant roles in plant innate immunity. *PLoS Pathogens* 5: e1000526.
- Moreno-Morcillo M, Minvielle-Sebastia L, Fribourg S, Mackereth CD. 2011. Locked tether formation by cooperative folding of Rna14p monkeytail and Rna15p hinge domains in the yeast CF IA complex. *Structure* 19: 534–545.
- Muskett PR, Kahn K, Austin MJ, Moisan LJ, Sadanandom A, Shirasu K, Jones JD, Parker JE. 2002. Arabidopsis RAR1 exerts rate-limiting control of R gene-mediated defenses against multiple pathogens. *Plant Cell* 14: 979–992.
- Naftelberg S, Schor IE, Ast G, Kornblihtt AR. 2015. Regulation of alternative splicing through coupling with transcription and chromatin structure. *Annual Review of Biochemistry* 84: 165–198.
- Niu D, Lii YE, Chellappan P, Lei L, Peralta K, Jiang C, Guo J, Coaker G, Jin H. 2016. miRNA863-3p sequentially targets negative immune regulator ARLPKs and positive regulator SERRATE upon bacterial infection. *Nature Communications* 7: 11324.
- van Nues RW, Beggs JD. 2001. Functional contacts with a range of splicing proteins suggest a central role for Brr2p in the dynamic control of the order of events in spliceosomes of *Saccharomyces cerevisiae*. *Genetics* 157: 1451–1467.
- Palma K, Zhang Y, Li X. 2005. An importin alpha homolog, MOS6, plays an important role in plant innate immunity. *Current Biology* 15: 1129–1135.
- Palma K, Zhao Q, Cheng YT, Bi D, Monaghan J, Cheng W, Zhang Y, Li X. 2007. Regulation of plant innate immunity by three proteins in a complex conserved across the plant and animal kingdoms. *Genes & Development* 21: 1484–1493.
- Raczynska KD, Stepień A, Kierzkowski D, Kalak M, Bajczyk M, McNicol J, Simpson CG, Szwejkowska-Kulinska Z, Brown JW, Jarmolowski A. 2014. The SERRATE protein is involved in alternative splicing in *Arabidopsis thaliana*. *Nucleic Acids Research* 42: 1224–1244.
- Rigo R, Bazin JRM, Crespi M, Charon CL. 2019. Alternative splicing in the regulation of plant–microbe interactions. *Plant & Cell Physiology* 60: 1906–1916.
- Selenko P, Gregorovic G, Sprangers R, Stier G, Rhani Z, Krämer A, Sattler M. 2003. Structural basis for the molecular recognition between human splicing factors U2AF65 and SF1/mBBP. *Molecular Cell* 11: 965–976.
- Shen Y, Zhou Z, Wang Z, Li W, Fang C, Wu M, Ma Y, Liu T, Kong LA, Peng DL *et al.* 2014. Global dissection of alternative splicing in paleopolyploid soybean. *Plant Cell* 26: 996–1008.
- Shi Y. 2017. Mechanistic insights into precursor messenger RNA splicing by the spliceosome. *Nature Reviews Molecular Cell Biology* 18: 655–670.
- Shirasu K, Lahaye T, Tan MW, Zhou FS, Azevedo C, Schulze-Lefert P. 1999. A novel class of eukaryotic zinc-binding proteins is required for disease resistance signaling in barley and development in *C. elegans*. *Cell* 99: 355–366.
- Staiger D, Brown JW. 2013. Alternative splicing at the intersection of biological timing, development, and stress responses. *Plant Cell* 25: 3640–3656.
- Takahashi A, Casais C, Ichimura K, Shirasu K. 2003. HSP90 interacts with RAR1 and SGT1 and is essential for RPS2-mediated disease resistance in Arabidopsis. *Proceedings of the National Academy of Sciences, USA* 100: 11777–11782.
- Tang F, Yang SM, Gao MQ, Zhu HY. 2013. Alternative splicing is required for RCT1-mediated disease resistance in *Medicago truncatula*. *Plant Molecular Biology* 82: 367–374.
- Thao NP, Chen L, Nakashima A, Hara S, Umemura K, Takahashi A, Shirasu K, Kawasaki T, Shimamoto K. 2007. RAR1 and HSP90 form a complex with Rac/Rop GTPase and function in innate-immune responses in rice. *Plant Cell* 19: 4035–4045.
- Tornero P, Merritt P, Sadanandom A, Shirasu K, Innes RW, Dangl JL. 2002. RAR1 and NDR1 contribute quantitatively to disease resistance in Arabidopsis, and their relative contributions are dependent on the R gene assayed. *Plant Cell* 14: 1005–1015.
- Van Nostrand EL, Pratt GA, Shishkin AA, Gelboin-Burkhart C, Fang MY, Sundararaman B, Blue SM, Nguyen TB, Surka C, Elkins K *et al.* 2016. Robust transcriptome-wide discovery of RNA-binding protein binding sites with enhanced CLIP (eCLIP). *Nature Methods* 13: 508–514.
- Wang BB, Brendel V. 2004. The ASRG database: identification and survey of *Arabidopsis thaliana* genes involved in pre-mRNA splicing. *Genome Biology* 5: R102.
- Wang ZP, Xing HL, Dong L, Zhang HY, Han CY, Wang XC, Chen QJ. 2015. Egg cell-specific promoter-controlled CRISPR/Cas9 efficiently generates homozygous mutants for multiple target genes in Arabidopsis in a single generation. *Genome Biology* 16: 144.
- Wiermer M, Palma K, Zhang Y, Li X. 2007. Should I stay or should I go? Nucleocytoplasmic trafficking in plant innate immunity. *Cellular Microbiology* 9: 1880–1890.
- Will CL, Luhrmann R. 2011. Spliceosome structure and function. *Cold Spring Harbor Perspectives in Biology* 3: a003707.
- Wu Z, Zhu D, Lin X, Miao J, Gu L, Deng X, Yang Q, Sun K, Zhu D, Cao X *et al.* 2016. RNA binding proteins RZ-1B and RZ-1C play critical roles in regulating pre-mRNA splicing and gene expression during development in Arabidopsis. *Plant Cell* 28: 55–73.
- Xie X, Ma X, Zhu Q, Zeng D, Li G, Liu YG. 2017. CRISPR-GE: a convenient software toolkit for CRISPR-based genome editing. *Molecular Plant* 10: 1246–1249.
- Xu F, Xu S, Wiermer M, Zhang Y, Li X. 2012. The cyclin L homolog MOS12 and the MOS4-associated complex are required for the proper splicing of plant resistance genes. *The Plant Journal* 70: 916–928.
- Xu SH, Zhang ZB, Jing BB, Gannon P, Ding JM, Xu F, Li X, Zhang YL. 2011. Transportin-SR is required for proper splicing of resistance genes and plant immunity. *PLoS Genetics* 7: e1002159.
- Yan C, Wan R, Shi Y. 2019. Molecular mechanisms of pre-mRNA splicing through structural biology of the spliceosome. *Cold Spring Harbor Perspectives in Biology* 11: a032409.
- Yang D, Zhao F, Zhu D, Chen X, Kong X, Wu Y, Chen M, Du J, Qu LJ, Wu Z. 2022. Progressive chromatin silencing of ABA biosynthesis genes permits seed germination in Arabidopsis. *Plant Cell* 34: 2871–2891.
- Yang SM, Tang F, Zhu HY. 2014. Alternative splicing in plant immunity. *International Journal of Molecular Sciences* 15: 10424–10445.

- Zhang M, Kadota Y, Prodromou C, Shirasu K, Pearl LH. 2010. Structural basis for assembly of Hsp90-Sgt1-CHORD protein complexes: implications for chaperoning of NLR innate immunity receptors. *Molecular Cell* 39: 269–281.
- Zhang S, Liu Y, Yu B. 2014. PRL1, an RNA-binding protein, positively regulates the accumulation of miRNAs and siRNAs in Arabidopsis. *PLoS Genetics* 10: e1004841.
- Zhang S, Xie M, Ren G, Yu B. 2013. CDC5, a DNA binding protein, positively regulates posttranscriptional processing and/or transcription of primary microRNA transcripts. *Proceedings of the National Academy of Sciences, USA* 110: 17588–17593.
- Zhang T, Lei J, Yang H, Xu K, Wang R, Zhang Z. 2011. An improved method for whole protein extraction from yeast *Saccharomyces cerevisiae*. *Yeast* 28: 795–798.
- Zhang XC. 2003. RPS4-mediated disease resistance requires the combined presence of RPS4 transcripts with full-length and truncated open reading frames. *Plant Cell* 15: 2333–2342.
- Zhang Y, Goritschnig S, Dong X, Li X. 2003. A gain-of-function mutation in a plant disease resistance gene leads to constitutive activation of downstream signal transduction pathways in suppressor of npr1-1, constitutive 1. *Plant Cell* 15: 2636–2646.
- Zhang YL, Cheng YT, Bi DL, Palma K, Li X. 2005. MOS2, a protein containing G-patch and KOW motifs, is essential for innate immunity in *Arabidopsis thaliana*. *Current Biology* 15: 1936–1942.
- Zhang YL, Li X. 2005. A putative nucleoporin 96 is required for both basal defense and constitutive resistance responses mediated by suppressor of npr1-1, constitutive 1. *Plant Cell* 17: 1306–1316.
- Zhu D, Mao F, Tian Y, Lin X, Gu L, Gu H, Qu LJ, Wu Y, Wu Z. 2020. The features and regulation of co-transcriptional splicing in Arabidopsis. *Molecular Plant* 13: 278–294.

Supporting Information

Additional Supporting Information may be found online in the Supporting Information section at the end of the article.

Dataset S1 List of primers used in this study.

Dataset S2 List of splicing-related proteins identified by IP-MS of AtSKRP.

Dataset S3 Information of alternative-splicing genes.

Fig. S1 Sequence conservation among SKRP homologs.

Fig. S2 Characterization of *atskrp* mutants.

Fig. S3 DAB staining and *PR5* detection of Arabidopsis infected by *Phytophthora capsici*.

Fig. S4 Self-interaction of AtSKRP as tested in different systems.

Fig. S5 Gel-filtration analysis of GST-AtSKRP that purified *in vitro*.

Fig. S6 Polymerization of AtSKRP is partially impaired in GFP-AtSKRPΔOR5 and GFP-AtSKRPΔOR10 mutant.

Fig. S7 Polymerization of GmSKRP is required for its immune repression activity.

Fig. S8 RNA-binding properties of AtSKRP.

Fig. S9 Failure of expression of PRR8 and BRR2 in yeast leads.

Fig. S10 The phenotype of *prp8*, *u2af65a*, *sr45* and *cdc5* in plant immunity against *Phytophthora capsici*.

Fig. S11 Genome Browser view of mRNA expression and GFP-AtSKRP-eCLIP at LNK2 and RAR1.

Fig. S12 Test of disease resistance of candidate proteins in *Nicotiana benthamiana*.

Fig. S13 Characterization of *ubp25* and *rar1*.

Fig. S14 Intron-splicing efficiency of *UBP25* and *RAR1* in *prp8* and *sr45* mutant.

Fig. S15 Accumulation of the unspliced RNA of *UBP25* and *RAR1* negatively impact plant immunity.

Methods S1 Callose deposition.

Methods S2 Yeast two-hybrid assays.

Methods S3 DAB staining.

Methods S4 GST-pull down.

Methods S5 Electrophoretic mobility shift assay.

Methods S6 *Agrobacterium*-mediated transient assay.

Methods S7 BiFC assay.

Methods S8 Gel filtration.

Methods S9 Polymer detection.

Methods S10 Yeast protein extraction.

Methods S11 RNA immunoprecipitation.

Methods S12 RNA isolation and RT-qPCR.

Methods S13 RNA sequencing library construction.

Methods S14 Motif discovery.

Please note: Wiley is not responsible for the content or functionality of any Supporting Information supplied by the authors. Any queries (other than missing material) should be directed to the *New Phytologist* Central Office.